UNIVERSITY OF SÃO PAULO

RIBEIRÃO PRETO MEDICAL SCHOOL

WILLIAN ROBERT GOMES

Immune mechanisms in hepatic and pulmonary fibrosis associated with telomeropathies in murine model and human disease

Ribeirão Preto
2024

WILLIAN ROBERT GOMES

Immune mechanisms in hepatic and pulmonary fibrosis associated with telomeropathies in murine model and human disease

Ph. D. Thesis presented to the Graduate Program in Clinical Oncology, Stem Cells and Cell Therapy at the Ribeirão Preto Medical School, University of São Paulo, to obtain the degree of Doctor of Science.

Concentration area: Normal and neoplastic differentiation.

Prof. Dr. Rodrigo do Tocantins Calado de Saloma Rodrigues.

Ribeirão Preto
2024

Gomes, Willian Robert.

Immune mechanisms in hepatic and pulmonary fibrosis associated with telomeropathies in murine model and human disease. Ribeirão Preto, 2024.

66 p. : il. ; 30cm.

Tese de Doutorado, apresentada à Faculdade de Medicina de Ribeirão Preto/USP – Área de concentração: Diferenciação normal e neoplásica.

Orientador: Calado, Rodrigo do Tocantins.

1. Telômeros. 2. Imunologia. 3. Fibrose. 4. Falência medular.

APPROVAL

Name: GOMES, Willian Robert.
Title: Immune mechanisms in hepatic and pulmonary fibrosis associated with telomeropathies in murine model and human disease.

Ph. D. Thesis presented to the Graduate Program in Clinical Oncology, Stem Cells and Cell Therapy at the Ribeirão Preto Medical School, University of São Paulo, to obtain the degree of Doctor of Science.

Approved in:

Examiners

Prof. Dr. _____

Institution: _____ Signature:_____

Prof. Dr. _____

Institution: _____ Signature:_____

Prof. Dr. _____

Institution: _____ Signature:_____

Prof. Dr. _____

Institution: _____ Signature:_____

ACKNOWLEDGEMENTS

I thank the funding agencies for supporting the development of this research - Coordination of Superior Level Staff Improvement (CAPES) and São Paulo Research Foundation (FAPESP), grants #2019/2500-2 and #2022/07634-4.

Special thanks to the Ribeirão Preto Medical School, Hospital das Clínicas de Ribeirão Preto, Blood Center of Ribeirão Preto and King's College London, for offering the necessary infrastructure and environment for the progress of this study. Also, I acknowledge the Graduate Program in Clinical Oncology, Stem Cells and Cell Therapy for the support.

To my advisor, Prof. Dr. Rodrigo Calado, who is a brilliant mentor and scientist, with whom I had the opportunity to learn and grow as a young researcher and a person.

To Prof. Ghulam Mufti, Dr. Giorgio Napolitani and Dr. Mohammad Karimi, from King's College London, who embraced our ideas and helped us from the very beginning until the completion of this thesis, offering crucial insights and thoughts.

To all professors who collaborated directly or indirectly with us – Dr. Leandra Ramalho, Dr. Lizandra Guimarães, Dr. Vanderlei Rodrigues, Dr. Vanessa Pereira, Dr. Marcelo Gomes, Dr. Antonio Condino-Neto, Dr. Edson Martinez and Dr. José Carlos Farias Filho.

To the lab specialists and technicians, for helping me with experiments and analysis – Bárbara, Rita, Deisy, Priscila, Josiane, Bete, Dalvinha and Julia from USP; Amandine, Riley and Martha from KCL.

To Cleide, Thamires and Beatriz, from the animal facility, for all the support, patience and for teaching everything I know about animal handling.

To Vinicius Silva, for being by my side in all experiments and attempts – in and out of the laboratory.

To all the other present and former members of our group, Flávia, Florencia, Luiz Fernando, Alexandre and Thiago.

To my family, especially my parents, sister and niece, for giving me the support and motivation to finish this work.

And, most importantly, I thank the volunteers who trusted us and accepted being part of this project.

Thank you very much.

“There is no science without fancy,
and no art without fact.” (Vladimir Nabokov, 1899-1977)

Resumo

GOMES, W.R. **Mecanismos imunes nas fibroses hepática e pulmonar associadas a telomeropatias em modelo murino e doença humana.** 2024. 66f. Tese (Doutorado). Faculdade de Medicina de Ribeirão Preto – Universidade de São Paulo, Ribeirão Preto, 2024.

Telômeros são estruturas complexas constituídas por sequências repetitivas de nucleotídeos que se associam a proteínas para formar as extremidades dos cromossomos lineares. A extensão telomérica reduz-se a cada ciclo mitótico e, quando os telômeros atingem comprimentos demasiadamente curtos, induzem as células a entrarem em senescência ou apoptose. Diferentes variantes patogênicas podem levar ao encurtamento excessivo dos telômeros, resultando no desenvolvimento de telomeropatias. A falência da célula-tronco hematopoética (anemia aplástica) é uma das principais manifestações clínicas das telomeropatias, porém pacientes podem desenvolver processos fibróticos em órgãos como os pulmões (fibrose pulmonar) e fígado (cirrose). Apesar de haver evidências que mostrem a correlação entre a erosão telomérica e a cirrose hepática, os mecanismos envolvidos neste processo não são bem compreendidos. O presente trabalho teve como objetivo avaliar os mecanismos imunes envolvidos no desenvolvimento de processo fibrótico hepático e pulmonar causado pelo encurtamento telomérico. Para isso, foram estudados modelos murinos nocaute *Terc*$^{-/-}$ e *Tert*$^{-/-}$ e animais selvagens com mesmo *background* genético foram avaliados como controles. A fibrose hepática foi induzida pela infecção controlada por *Schistosoma mansoni*. Após 12 semanas de infecção, os animais foram sacrificados para coleta de amostras. O índice de fibrose hepática foi determinado por *Picro-Sirius Red*, e a caracterização fenotípica dos macrófagos infiltrados foi realizada por imunoistoquímica. Macrófagos derivados da medula óssea foram testados quanto à sua capacidade de polarização *in vitro*. No soro, o perfil de citocinas foi avaliado por CBA para identificação das vias inflamatórias envolvidas. Adicionalmente, também foram estudados pacientes portadores de telomeropatias com fibrose pulmonar e/ou cirrose diagnosticadas por métodos de imagem e/ou biópsia. A caracterização fenotípica e estratificação das subpopulações de linfócitos T, B, NK, monócitos e células dendríticas em sangue periférico foi realizada por citometria de massas (CyTOF) e o padrão de citocinas séricas foi determinado por Luminex a fim de se verificar as diferenças exibidas no perfil imune celular e molecular nos pacientes que desenvolvem doença fibrótica. Os resultados mostram que o silenciamento de *Terc* ou *Tert* causa alterações na capacidade de resposta imune em camundongos, especialmente em macrófagos, que culminam em redução da resposta fibrótica pós-infecção com *S. mansoni*. Pacientes apresentam subpopulações pró-inflamatórias e com fenótipo senescente, além de variações em citocinas, quimiocinas e fatores de crescimento causadas pelas citopenias. Espera-se que os resultados contribuam para a melhor compreensão de como as disfunções teloméricas influenciam no desenvolvimento de processos fibróticos, e que possíveis novos alvos terapêuticos sejam identificados para tratamento destas complicações.

Palavras-chave: Telômeros. Imunologia. Fibrose. Falência medular.

Abstract

GOMES, W.R. **Immune mechanisms in hepatic and pulmonary fibrosis associated with telomeropathies in murine model and human disease.** 2024. 66p. Thesis (Ph. D). Ribeirão Preto Medical School – University of São Paulo, Ribeirão Preto, 2024

Telomeres are complex structures made up of repetitive sequences of nucleotides associated with proteins to form the ends of linear chromosomes. Telomere length reduces with each mitotic cycle and, once excessively short, they induce cells to engage senescence or apoptosis. Different pathogenic variants can lead to excessive shortening of telomeres, resulting in the development of telomeropathies. Hematopoietic stem cell failure (aplastic anemia) is one of the main clinical manifestations of telomeropathies, but patients might develop fibrotic responses in organs such as the lungs (pulmonary fibrosis) and liver (cirrhosis). Although there is evidence showing correlation between telomeric erosion and liver cirrhosis, the mechanisms involved in this process are not well understood. The present work aimed to evaluate the immune mechanisms involved in the development of hepatic and pulmonary fibrotic processes caused by telomeric shortening. For this, *Terc*$^{-/-}$ and *Tert*$^{-/-}$ knockout murine models were studied and wild-type animals with the same genetic background were evaluated as controls. Liver fibrosis was induced by controlled *Schistosoma mansoni* infection. After 12 weeks of infection, animals were sacrificed for sample collection. Liver fibrosis index was determined by Picro-Sirius Red, and phenotypic characterization of infiltrated macrophages was performed by immunohistochemistry. Bone marrow-derived macrophages were tested for their polarization capacity in vitro. In serum, the cytokine profile was evaluated by CBA to identify the inflammatory pathways involved. Additionally, patients with telomeropathies and pulmonary fibrosis and/or cirrhosis, diagnosed by imaging and/or biopsy, were also studied. The phenotypic characterization and stratification of subpopulations of T, B, NK lymphocytes, monocytes and dendritic cells in peripheral blood was performed by mass cytometry (CyTOF) and the serum cytokine profile was determined by Luminex in order to verify the differences displayed in the cellular and molecular immune profile in patients who develop fibrotic disease. Results show that *Terc* or *Tert* silencing causes changes in the immune response capacity in mice, especially in macrophages, which culminate in a reduction in the fibrotic response following the infection with *S. mansoni*. Patients present with pro-inflammatory subpopulations and a senescent phenotype, in addition to variations in cytokines, chemokines and growth factors caused by cytopenias. It is expected that the results will contribute to a better understanding of how telomeric dysfunctions influence the development of fibrotic processes, and that possible new therapeutic targets will be identified for the treatment of these complications.

Keywords: Telomeres. Immunology. Fibrosis. Bone marrow failure.

INDEX

1. INTRODUCTION

Telomeres are ribonucleoprotein complexes at the end of linear chromosomes whose function is to maintain the integrity of the genetic material. They consist of repeating hexanucleotide sequences of 5'-TTAGGG-3' associated with at least six shelterin proteins (POT1, RAP1, TIN2, TPP1, TRF1 and TRF2), that maintain the structure stability (LU et al., 2013; PALM; DE LANGE, 2008).Such proteins facilitate the formation of a loop-shaped structure, or t-loop, which recovers the chromosomal ends and protects them against damage and strand breaks (CARVALHO; GOMES; CALADO, 2022). Telomeres shorten with each mitotic division, as DNA polymerase is unable to completely replicate the 3' ends of chromosomes (SHAY; WRIGHT, 2019). Once critically short, the t-loop structure of telomeres is lost and the chromosomal end becomes recognizable as DNA strand breakage by cellular repair mechanisms, activating apoptosis or senescence signaling pathways (AUBERT; LANSDORP, 2008). However, in cells with high proliferative activity, such as embryonic and adult stem cells, telomeric loss is attenuated by the activity of telomerase, a reverse transcriptase holoenzyme that catalyzes the addition of new nucleotide sequences to telomeres (AUBERT; LANSDORP, 2008; LU *et al.*, 2013)

The telomerase complex includes a reverse transcriptase enzyme (TERT), the RNA component (TERC), which serves as a template for telomere lengthening, and proteins responsible for stabilizing the complex, notably dyskerin (DKC1), GAR1 (H/ACA ribonucleoprotein complex subunit 1), NHP2 (H/ACA ribonucleoprotein complex subunit 2), NOP10 (H/ACA ribonucleoprotein complex subunit 3) and TCAB1 (telomerase Cajal body protein 1) (CARVALHO; GOMES; CALADO, 2022; SHAY; WRIGHT, 2019) (Figure 1). Different germline variants can impair the functionality of the telomere-telomerase complex and lead to the occurrence of a group of diseases called telomere-biology disorders (TBDs), or telomeropathies, characterized mainly by the abnormal and premature shortening of telomeres (CALADO; YOUNG, 2009). One of the first studies to indicate that short telomeres are associated with disease was published by Ball and colleagues (1998), in which telomeric shortening of leukocytes was observed in patients with aplastic anemia. Disease duration was related to telomere length. However, it was not clear whether telomere erosion was a cause or consequence of bone marrow failure. The identification of pathogenic variants in the

DKC1 gene, which encodes dyskerin, in patients with dyskeratosis congenita (DC), determined causality (HEISS, 1998).

Figure 1. Telomere structure

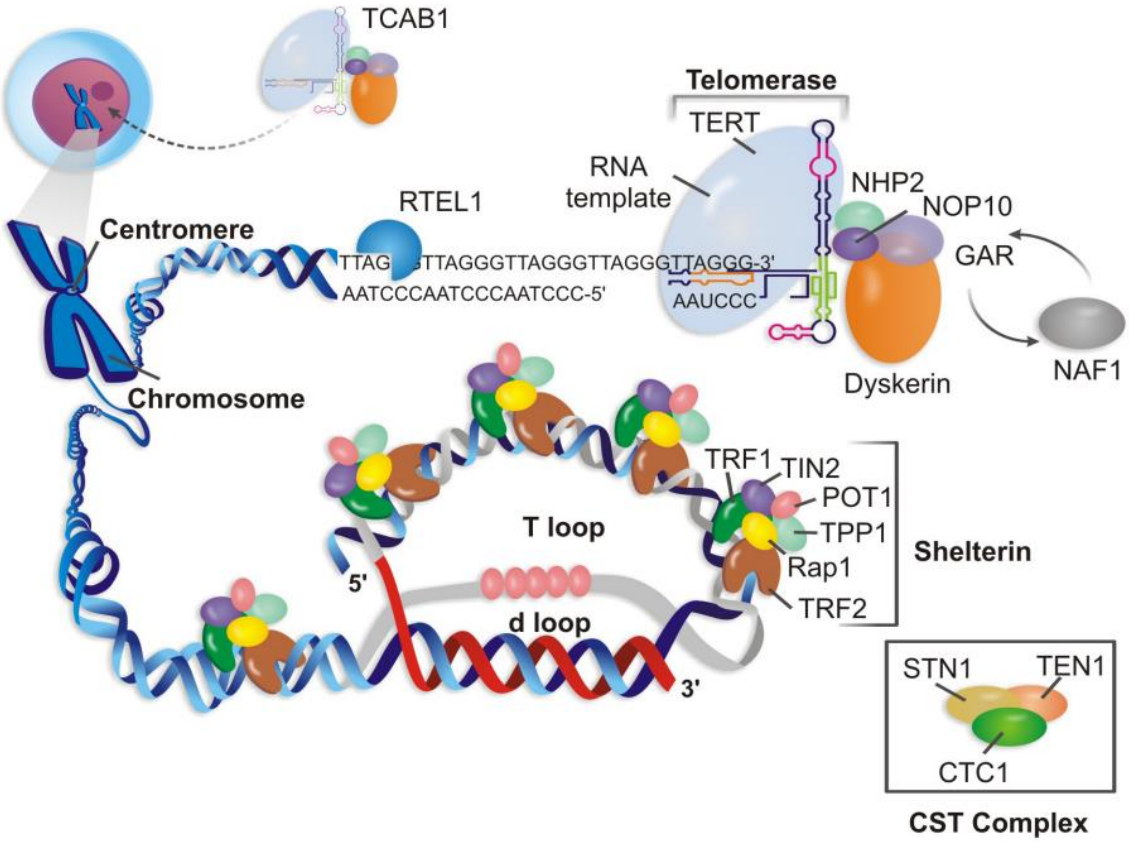

Source: Carvalho, Gomes & Calado, 2022

Considered as the prototype of telomeropathies, DC is a rare disease, and its inheritance might be autosomal dominant, recessive or linked to the X chromosome (region Xq28), caused mainly by germline variants in *TINF2* or *DKC1* (HEISS, 1998; SAVAGE, 2018). However, TBDs are associated with variants in at least 16 genes involved in telomere biology: components of the telomerase complex (*DKC1*, *TERC*, *TERT*, *NOP10*, and *NHP2*), shelterins (*ACD*, *TINF2*, and *POT1*), proteins of telomere coverage (*CTC1* and *STN1*) and proteins that interact directly or indirectly with telomeric maintenance (*RTEL1*, *NAF1*, *WRAP53*, *USB1*, *ZCCHC8* and *PARN*) (CARVALHO; GOMES; CALADO, 2022). Due to impaired telomere maintenance, TBD patients have very short telomeres with stem cell exhaustion and tissue failure (BERTUCH, 2016; HOLOHAN; WRIGHT; SHAY, 2014). Bone marrow is particularly

affected, with 80% of patients developing bone marrow failure (BMF) (GRAMATGES; BERTUCH, 2013; PAIVA; CALADO, 2014).

BMF is the most recurrent manifestation of telomeropathies in children, while in adults IPF is a frequent cause of mortality (FERNÁNDEZ GARCÍA; TERUYA-FELDSTEIN, 2014). This complication is a specific form of fibrosing interstitial pneumonia, characterized by diffuse and progressive remodeling of the lung parenchyma, with deposition of extracellular matrix and irreversible scarring (BILGILI et al., 2019a; CALADO; YOUNG, 2009; MOLINA-MOLINA; BORIE, 2018). The histopathological and/or radiological pattern associated with IPF is usual interstitial pneumonia (UIP), determined by reticular abnormalities with basal and subpleural predominance, honeycombing, involvement of the lung parenchyma by fibrotic tissue and the presence of fibroblastic foci (BILGILI et al., 2019b; MARTINEZ et al., 2017). The mechanisms that lead to the development of IPF in patients with TBDs remain uncertain, but telomeric erosion seems to dampen tissue repair (ARISH; PETUKHOV; WALLACH-DAYAN, 2019).

The cellular type affected by telomeric shortening plays an important role in the occurrence of IPF. Naikawadi et al., (2016) demonstrated that silencing *Trf1* in fibroblasts and type I collagen-secreting cells from mouse lungs, leads to pulmonary edema, but not fibrosis. In contrast, *Trf1* silencing in type II alveolar epithelial cells culminates in tissue remodeling and spontaneous pulmonary fibrosis, in addition to promoting the recruitment of macrophages and an increase in TGF-β1. Suppression of the *Trf1* gene leads to telomeric shortening in the cells tested. Similarly, Povedano et al., 2015)reported that deletion of the *Trf1* gene in type II alveolar cells induces DNA damage, macrophage infiltration in lung tissue, and lesions compatible with IPF in mice. The involvement of this cell type is also relevant in IPF in humans. Telomere shortening is predominantly observed in type II alveolar cells, which is associated with the presence of fibrotic lesions. This cell population appears to be essential for effective lung tissue repair, and telomeric loss directly impairs this mechanism (BILGILI et al., 2019b; SISSON et al., 2010).

Hepatic disease is also a clinical manifestation that occurs in approximately 7% of patients with DC, with fibrosis (and subsequent progression to cirrhosis) and regenerative nodular hyperplasia of the liver (CALADO et al., 2011; KIRWAN; DOKAL, 2009) However, the connection between these two conditions has not yet been completely elucidated. Cirrhosis is the final and irreversible stage of liver disease,

characterized by a diffuse alteration of the organ and the replacement of its normal architecture by regenerative nodules together with the production of fibrotic tissue, which culminates in the reduction of liver function, portal hypertension and increased risk for hepatocellular carcinoma (GIULIO ROMANELLI; STASI, 2016; TSOCHATZIS; BOSCH; BURROUGHS, 2014). Cirrhosis is divided in two clinical phases: compensated and decompensated. In the first, the disease is asymptomatic, and the portal pressure is still normal or low enough so that ascites and other complications do not appear. The decompensated phase, on the other hand, occurs when portal hypertension becomes unsustainable, leading to the development of ascites, abdominal varicose veins, hepatic encephalopathy, jaundice, among other possible complications (GIULIO ROMANELLI; STASI, 2016).

The development of liver cirrhosis is triggered by a complex chain of processes mediated by inflammatory cytokines that regulate the activation of hepatic stellate cells (HSCs) and tissue fibrogenesis. HSCs, or perisinusoidal cells, play an important role in the pathophysiology of cirrhosis. These cells, whose main function is to store vitamin A, are present in the space between the sinusoidal capillaries and the hepatocytes, also known as space of Disse (FRIEDMAN, 2000) HSCs secrete several substances that act on hepatocytes, such as growth factors, cytokines, prostaglandins and, in response to liver injury, these cells can be activated and transform into contractile myofibroblasts capable of synthesizing extracellular matrix, such as collagen, proteoglycans and glycoproteins (FRIEDMAN, 2000; GANDHI, 2015). The activation of HSCs and the acquired contractile characteristic increase the vascular resistance of the sinusoids and activated HSCs show a decreased response to vasodilators, such as nitric oxide (IWAKIRI, 2014; PERRI et al., 2006)). Another consequence is the process of angiogenesis, in which new blood vessels are formed around regenerative nodules and fibrotic septa due to the secretion of angiogenic factors such as angiopoietin and vascular endothelial growth factor, or VEGF, by these cells (IWAKIRI, 2014; NOVO et al., 2007; TAURA et al., 2008; THABUT et al., 2011).

The most potent mitogen of HSCs is platelet-derived growth factor (PDGF), whose activity increases proportionally to the degree of liver fibrosis (CAO et al., 2010; MARTIN et al., 2013; THIERINGER et al., 2008). Several factors, such as viral infections, xenobiotics or mechanical damage to hepatocytes, may trigger the synthesis and secretion of PDGF by Kupffer cells, which are resident macrophages of liver tissue implicated in the pathogenesis of different liver diseases (ZHOU; ZHANG;

QIAO, 2014). Concomitantly, activated HSCs, Kupffer cells, hepatocytes and sinusoidal endothelial cells begin to secrete transforming growth factor beta, or TGF-β, considered the main inducer of fibrogenesis in the process of liver fibrosis (ZHOU; ZHANG; QIAO, 2014). TGF-β initiates its pro-fibrotic effect by stimulating HSCs which, in turn, also begin to secrete the cytokine in an autocrine manner (GANDHI, 2017; WELLS; KRUGLOV; DRANOFF, 2004). TGF-β also induces the expression of genes responsible for the production of extracellular matrix and suppresses metalloproteinases (MMPs), important enzymes in the degradation of collagen, fibronectin, elastin and other matrix components (CUI et al., 2011; LIU; HU; YIN, 2006).

Interleukins (ILs) also influence the process of liver fibrosis and cirrhosis, being secreted mainly by T lymphocytes, monocytes, macrophages and endothelial cells in response to an inflammatory process (ZHOU; ZHANG; QIAO, 2014). In fibrogenesis, ILs can be divided into pro-fibrotic and anti-fibrotic. In the first class, there are IL-1 and IL-17, which act, above all, in the positive regulation of the synthesis of extracellular matrix and in the induction of chronicity of the inflammatory process (DU et al., 2013; GIELING; WALLACE; HAN, 2009; KAMARI et al., 2011; PETRASEK et al., 2012). On the other hand, the fibrogenesis process can be attenuated by cytokines such as IL-10 and IL-22, which inhibit the activation of HSCs, induce the senescence of myofibroblasts and inhibit the synthesis of mediators such as TGF-β and MMPs (KHAWAR et al., 2016; SZIKSZ et al., 2015). Furthermore, IL-6 is capable of attenuating apoptosis and promoting hepatocyte regeneration, reducing tissue damage (NASEEM; HUSSAIN; MANZOOR, 2018).

Persistent chronic inflammation in fibrotic processes leads to tissue infiltration of mononuclear cells (BARRON; WYNN, 2011; WYNN, 2011). $CD4^+$ T lymphocytes play a fundamental role in the development and progression of fibrosis. Liver fibrosis is closely linked to the response of T_H2 lymphocytes, involved in the secretion of pro-fibrotic inflammatory mediators, such as IL-4, IL-5, IL-13 and IL-21 (GIESECK; WILSON; WYNN, 2018; WYNN, 2008). On the other hand, cytokines associated with the T_H1 response, such as gamma interferon (IFN-γ) and IL-12, have anti-fibrotic properties (PAUN; BERGERON; HASTON, 2017).

The polarization of the lymphocyte response to T_H1 or T_H2 induces the expression of distinct gene profiles in experimental models of fibrosis. Hoffmann and collaborators (2001) studied the inflammatory response induced by *Schistosoma mansoni* infection in mice genetically modified to present immunological profiles

polarized towards T_H1 or T_H2. T_H1^+/T_H2^- animals showed low collagen deposition in the liver and had greater expression of pro-apoptotic genes, in addition to IFN-γ. On the other hand, T_H2-polarized mice suffered excessive collagen deposition in liver tissue and high expression of pro-fibrotic genes, such as procollagen, lysyl oxidase and fibrillin, corroborating the T_H2 response hypothesis (KAMINSKI et al., 1999; SANDLER et al., 2003; ZHANG et al., 2017).

Several conditions increase the risk of cirrhosis, such as viral hepatitis, alcohol abuse and steatosis. Furthermore, genetic factors, such as telomeric shortening, are identified as possible modulators (CARULLI, 2015; LAISH, 2019).Kitada and colleagues (1995) demonstrated a progressive decrease in telomeres in hepatocytes from patients with chronic hepatitis and cirrhosis: shorter telomeres were observed in hepatocytes from patients at a more advanced stage. Other authors found similar patterns of progressive telomere shortening, suggesting an association with the progression of chronic hepatitis to cirrhosis and even hepatocellular carcinoma (MIURA et al., 1997; PLENTZ et al., 2004; WIEMANN et al., 2002). In the study conducted by Rudolph et al. (2000) with *Terc*$^{-/-}$ mice, administration of carbon tetrachloride (CCl_4) led to the development of cirrhosis in a more pronounced manner compared to wild-type (WT) animals. Reactivating telomerase in the liver reduced organ damage and promoted improvement in the organ's function. However, it is worth highlighting that, despite being widely used, the CCl_4-induced liver fibrosis model has some limitations, such as the variation in susceptibility in different strains of mice, the high mortality rate and reproducibility that is not always satisfactory (FORTEA et al., 2018; SCHOLTEN et al., 2015).

The presence of germline pathogenic variants in telomerase genes in patients with cirrhosis was described concomitantly by two groups. Calado et al., (2011) investigated variants in the *TERC* and *TERT* genes, in 134 patients diagnosed with cirrhosis. The frequency of variants in *TERT* was significantly higher in cirrhotic patients. Cirrhosis has also been correlated with shorter telomeres in peripheral blood leukocytes. In a similar study, Hartmann et al., (2011) performed the sequencing of *TERC* and *TERT* in 521 patients with cirrhosis. There was a higher occurrence of variants in the group with cirrhosis. Donaires and colleagues (2017) reported a higher frequency of *TERT* variants in 120 patients with hepatocellular carcinoma secondary to cirrhosis.

Short telomeres caused by loss-of-function variants in telomerase are also associated with alterations in the cytokine-mediated immune response in animal models. *Terc*$^{-/-}$ mice present a higher concentration of TGF-β and greater activation of the TGF-β/Smads pathway in lung tissue when subjected to treatment with lipopolysaccharide and bleomycin for the induction of IPF (LIU et al., 2018). This signaling pathway is related to multiple functions, including the regulation of the immune response, inflammation and cell differentiation (YAO LAN et al., 2011). Chen et al., (2015) showed that *Terc*$^{-/-}$ and *Tert*$^{-/-}$ mice have increased IL-1, IL-6, CXCL15 (homologue of human IL-8), IL-10, tumor necrosis factor α (TNF -α) and monocyte chemotactic protein (CCL2). On the other hand, there was a reduction in TGF-β in the knockout animals compared to the WT group. Additionally, it was observed that hepatocytes from *Tert*$^{-/-}$ mice have abnormal metabolic function (ALVES-PAIVA et al., 2018). When subjected to a high-fat diet, these animals developed liver lesions with the presence of steatosis, dysregulation of oxidative phosphorylation pathways and impairment of mitochondrial functions.

Although there is evidence of an association between telomeric maintenance deficiency and the development of fibrotic processes, the cellular and molecular mechanisms are poorly understood. Although telomeric erosion leads to cellular senescence, which impairs tissue regeneration, senescence per se does not fully explain the fibrogenic response. The present study aimed to investigate the cellular and molecular mechanisms involved in the development of fibrosis resulting from telomeric dysfunction. For that, murine models were used, with evaluation of the cellular immune profile in *Terc*$^{-/-}$ and *Tert*$^{-/-}$ mice subjected to experimental induction of cirrhosis by infection with *S. mansoni*. Likewise, patients diagnosed with telomeropathies were evaluated for activated inflammatory pathways in the concomitant presence of liver and/or lung fibrosis.

2. OBJECTIVES

2.1. General

To evaluate cellular and molecular immune profiles in murine models and patients with short telomere syndromes, with or without concomitant fibrosis.

2.2. Specific

2.2.1. Murine model

i) To induce liver fibrosis in *Terc*$^{-/-}$ and *Tert*$^{-/-}$ mice and evaluate collagen deposition and inflammatory cells infiltration;

ii) To identify macrophage phenotypes in fibrotic liver and investigate the polarization of bone marrow-derived macrophages (BMDMs) in vitro;

iii) To analyze the cytokine profile in plasma of mice with hepatic fibrosis.

2.2.2. Humans

i) To identify TBD patients with clinical manifestations, including or not lung and/or liver fibrosis, seen at the Blood Center of Ribeirão Preto – Ribeirao Preto Medical School, University of São Paulo (FMRP-USP);

ii) To determine immune cell subsets in peripheral blood, by mass cytometry (CyTOF);

iii) To evaluate serum levels of cytokines, chemokines and growth factors by Luminex™.

3. METHODS

3.1. Murine model

3.1.1. Colonies of knockout mice

Knockout mice for *Tert* and *Terc* plus WT mice (C57BL6/J background), housed at the animal facility from the Blood Center of Ribeirão Preto - USP and originally obtained from The Jackson Laboratory (JAX, Bar Harbor, Maine, USA), were kept in cages under standardized conditions of temperature (22 to 23 °C) and luminosity (12h/12h). Since telomeric shortening is accentuated after successive breeding, it was established that third-generation knockout animals (G3) would be used, as described in previous studies (AR et al., 2016a; PIÑEIRO-HERMIDA et al., 2020). For this, heterozygous *Terc*$^{+/-}$ or *Tert*$^{+/-}$ mice were intercrossed to generate G1 *Terc*$^{-/-}$ or *Tert*$^{-/-}$ mice. Animals from the same offspring were intercrossed to give rise to G2 *Terc*$^{-/-}$ or *Tert*$^{-/-}$, which were then used to give rise to G3 mice. Furthermore, WT mice from both

colonies were used as a control group. Upon reaching eight weeks of age, male and female mice were separated to be used in the study. Animal use was approved by the Local Ethics Committee (protocol 244/2019; Attachment A).

3.1.2. Genotyping

Newborn mice, from 10 to 15 days old, underwent tissue fragment collection through ear punching. Fragments were stored in microtubes and frozen at -20 °C until DNA extraction. DNA extraction was performed by lysis in alkaline solution. First, 200 µL of 50 mM sodium hydroxide (NaOH) were added to the microtubes containing the biological material, with subsequent incubation at 95-100 ºC for 1 hour. Then, 50 µL of 1 M Tris-hydrochloric acid (Tris-HCl), pH 6.8, were added to neutralize the reaction. After vortexing, the tubes were centrifuged at 4000 rpm for 3 minutes and used immediately for genotyping, or stored at -20 °C for later use.

Genotyping was carried out using the Polymerase Chain Reaction (PCR), with specific primers for the genes of interest. The primers used for *Tert* genotyping had the following sequences: 5'-CCCCAGGCGCCGCACAAAGG-3' (common forward); 5'-GGTCCTGGCTGTTTTCTAAG-3' (WT reverse); 5'-CTGGATTCATCGACTGTGGC-3' (mutant reverse). The primers used for *Terc* genotyping had the following sequences: 5'-AGTGTCTCGGTGCCTTGACT-3' (WT forward); 5'-TACCGGTGGATGTGGAATGT-3' (mutant forward); 5'-GTGATGTTGAGTTCCCACAG-3' (mutant reverse).

PCR products were applied to a 1.5% agarose gel containing ethidium bromide and analyzed on a UV transilluminator. Figure 2 displays the expected banding patterns. For *Tert*, WT samples present fragments of 150 base pairs (bp), while the mutant genotype (knockout) presents fragments of 420 bp. Heterozygotes should present both bands. For *Terc*, WT samples present fragments of 367 bp, while the mutant genotype (knockout) presents fragments of 196 bp. Heterozygotes must present both bands. 1000 bp (or 1 kb) markers were used.

Figure 2. Banding profiles of *Terc* and *Tert* genotyping in agarose gel.

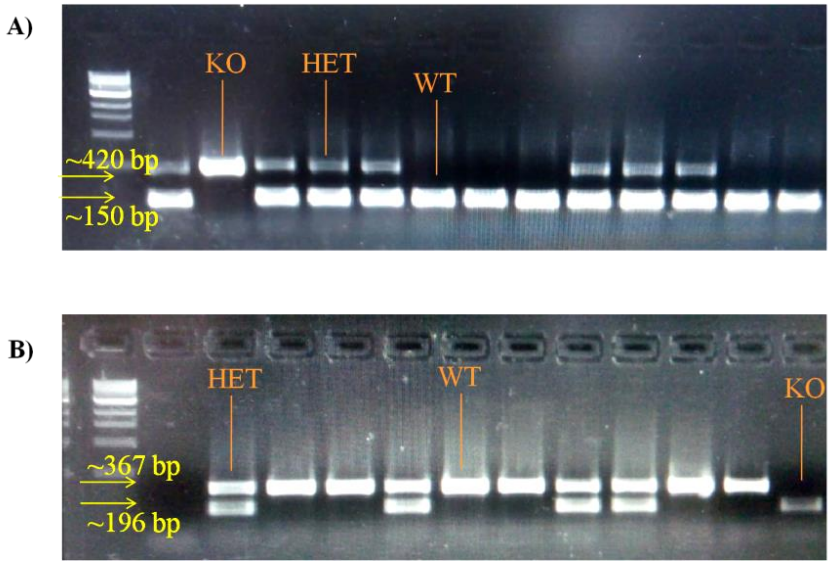

Banding profiles obtained from the genotyping of *Terc* and *Terc* genes in mice. **(A)** *Tert* genotyping. **(B)** *Terc* genotyping.

3.1.3. Induction of hepatic inflammation

To induce liver inflammation, mice were infected with *S. mansoni* through subcutaneous interscapular injection of approximately 100 cercariae per animal. The animals were anesthetized with inhaled isoflurane during the procedure. *S. mansoni* cercariae were provided by the Parasitology Research Laboratory of the University of Franca (Unifran), coordinated by Prof. Dr. Lizandra Guidi Guimarães, and by the Parasitology Laboratory at FMRP-USP, coordinated by Prof. Dr. Vanessa Carregaro Pereira and Prof. Marcelo Damário Gomes, where the parasite cycle is maintained in *Biomplaharia glabrata* snails and BALB/c mice. At the same time, uninfected animals were kept under the same conditions to be used as a control group. Table 1 provides details about the animal groups.

The infection time used in the present study was 12 weeks post-inoculation, to evaluate the chronic phase of infection (CHEEVER et al., 2002; CRESPO YANGUAS et al., 2016). After this period, mice were sacrificed with an overdose of ketamine and xylazine (300 and 30 mg/kg, respectively) intraperitoneally. Blood samples were collected via cardiac puncture in microtubes containing heparin, to obtain whole blood and plasma. The left lateral hepatic lobe was separated and sectioned into 0.5 cm thick fragments, with subsequent fixation in 10% formalin solution, in PBS buffer. Fragments of approximately 30 mg were sectioned from the remaining hepatic portions, stored in

cryovials and immediately frozen in liquid nitrogen for subsequent DNA extraction. Similarly, spleen biopsies were embedded in 10% formalin and frozen in liquid nitrogen; the left lung was sectioned in half, and both fragments were fixed in formalin.

Table 1. Animal groups included in the study.

	Infected	***Not infected***
Wild type	**12**	**20**
Male	07	08
Female	05	12
***Terc*$^{-/-}$**	**16**	**13**
Male	09	05
Female	07	08
***Tert*$^{-/-}$**	**16**	**18**
Male	08	08
Female	08	10

3.1.4. DNA extraction from peripheral blood and liver fragments

Peripheral blood samples (approximately 1 mL) were lysed in erythrocyte lysis solution for 10 minutes at 4 °C, and then leukocytes were washed in PBS and lysed in Puregene Cell Lysis Solution for, at least, 24h (#158116, Qiagen, California, USA). Proteins were precipitated and the supernatant was transferred to a new microtube, where isopropanol was added for nucleic acid precipitation. Following high-speed centrifugation, DNA pellet was washed with 70% ethanol and then resuspended in hydrating solution. Liver fragments, of approximately 30 mg, were used for DNA extraction with the DNeasy Blood & Tissue Kit (#69506, Qiagen, California, USA), according to the manufacturer's instructions.

DNA concentration and quality were assessed in a spectrophotometer.

3.1.5. Telomere length measurement

The telomere length (TL) of mouse leukocytes and liver were determined using the qPCR technique. Reactions included genomic DNA extracted from leukocytes or liver fragments (1.6 ng), RotorGene SYBR Green 2X, RNAse-free ultrapure water,

primer Tel forward (300 nM) (5'-CGGTTTGTTTGGGTTTGGGTTTGGGTTTGGGTTTGGGTT-3') and Tel reverse (300 nM) (5'- GGCTTGCCTTACCCTTACCCTTACCCTTACCCTTACCCT-3'), or primer for the forward single-copy gene (m36B4) (5'-GCTCCAAGCAGATGCAGCA-3') and reverse single-copy gene (5'- CCGGATGTGAGGCAGCAG-3'), in a total volume of 24 µL. The qPCR reactions were prepared in triplicate using the QIAgility automatic pipettor (Qiagen, California, USA), and amplification was carried out in the RotorGene-Q thermocycler (Qiagen).

Telomeric length was calculated by the telomere/single copy gene ratio (T/S ratio), which comprises ΔCt [Ct(telomere)/Ct(single gene)]. The T/S ratio for each sample (x) was normalized by the average T/S of a reference sample (ref), which was obtained from a pool of five random WT samples [$2\text{-}(\Delta Ct_x \times 2\Delta Ct_{Ref})=2^{-\Delta\Delta Ct}$]. The reference sample was also used to prepare a standard curve (10 ng; 5 ng; 2.5 ng; 1.25 ng; 0.625 ng; 0.132 ng).

3.1.6. Histopathological analysis of liver samples

Liver tissue biopsies collected after euthanasia of the mice were kept in a 10% formalin solution for a period of 48h, and then subjected to dehydration with 70% ethanol, clarification with xylene and subsequent inclusion in paraffin. The histological sections, measuring 5 µm, were stained with hematoxylin-eosin (HE), for histopathological analysis regarding the presence of granulomas in the tissue, and Picro-Sirius Red, which highlights the deposition of collagen in the tissue through the reddish color of the fibers (JUNQUEIRA; BIGNOLAS; BRENTANI, 1979). The fibrotic density index was calculated as the ratio between the area occupied by collagen fibers and the total area of the microscopic field, at 400× magnification. Calculations were performed using ImageJ software (ImageJ, 1.33u, NIH, USA).

Liver tissue was also used in immunohistochemical analyzes to phenotypically identify macrophages present in the cellular infiltrate, according to methodology described by Komohara et al., (2017). Histological sections were treated with blocking solution (bovine serum albumin, BSA) and subsequently incubated with the primary antibodies of interest: F4/80, CD68, iNOS and CD206. Slides were washed with PBS, incubated with secondary antibody and reactions were revealed with diaminobenzidine (DAB). Slides were counterstained with hematoxylin. Positively labeled cells were

counted with the aid of ImageJ 1.33u software (NIH, USA). Blind histopathological analyzes were carried out by an independent pathologist (Prof. Dr. Leandra Zambelli Ramalho – Department of Pathology at FMRP-USP).

3.1.7. Determination of cytokines in plasma from infected mice

Plasma samples obtained from the infected groups of mice were used for the measurement of IFN-γ, TNF-α, IL-2, IL-4, IL-6, IL-10 and IL-17A. Determinations were performed using the BD Cytometric Bead Array (CBA) Mouse Th1/Th2/Th17 Cytokine Kit (#560485, BD Biosciences), according to the manufacturer's instructions. Analysis was performed using FlowJo™ v.10.9.0 software (BD Biosciences). Samples were used undiluted for this analysis.

3.1.8. In vitro polarization of bone marrow-derived macrophages

BMDMs were isolated from a second group of animals (n = 12; 4 animals per group, eight to twelve weeks old), and cultured as previously described by YING et al., (2013) and (WANDERLEY et al., 2018). Cells were obtained from maceration of the femur and tibia, with subsequent filtration in a 100 µm cell strainer and cultivation in RPMI-1640 medium containing 10% fetal bovine serum (FBS) and 20% of L929 cell culture supernatant, rich in macrophage colony-stimulating factor (M-CSF). Cultures were maintained for 7 days, at 37 ºC and 5% CO2, with change of medium in every 3 days. After initial differentiation, macrophage polarization was stimulated with the addition of specific components: complete RPMI medium (negative control - M0), RPMI medium plus 100 ng/mL of lipopolysaccharide (LPS; M1-like polarization) or 10 ng/mL of IL-4 (M2-like). After incubation for 24 hours, cell polarization was assessed by nitrite quantification through Griess assay and gene expression for *Tnf-α*, *Mmp9*, *Il-6, Cd206* and *Arg1*, by RT-PCR, using *Gapdh* as reference gene. Expression ratio was calculated based on each primer's efficiency (from 90-110%). Primer sequences are listed on Chart 1.

Chart 1. Primers used for gene expression of BMDMs.

Gene	Forward	Reverse
Arg1	5'-CCAGAAGAATGGAAGAGTCAGTGT-3'	3'-GCAGATATGCAGGGAGTCACC-5'
Cd206	5'-CTCGTGGATCTCCGTGACAC-3'	3'-GCAAATGGAGCCGTCTGTGC-5'
Gapdh	5'-GGGTGTGAACCACGAGAAAT-3'	3'-CCTTCCACAATGCCAAAGTT-5'
Il-6	5'-TTCCTACCCCAATTTCCAAT-3'	3'-CCTTCTGTGACTCCAGCTTATC-5'
Mmp9	5'-AACATCTGGCACTCCACACC-3'	3'-GCAGAAGTTCTTTGGCCTGC-5'
Tnf-a	5'-GGTGCCTATGTCTCAGCCTCTT-3'	3'-GCCATAGAACTGATGAGAGGGAG-5'

3.1.9. Statistical analysis

Data from the different experimental groups were compared by ANOVA or Kruskal-Wallis, depending on data normality and distribution, assessed by Shapiro-Wilk test. When applicable, two-group comparisons were performed by either Mann-Whitney or Student's *t* test (with Welch's correction if necessary). Spearman correlations were also conducted. *p*-values of ≤0.05 were considered significant. GraphPad Prism v.9.5.1 (GraphPad Software, Boston, Massachusetts, USA) was used to analyze the data.

3.2. TBD patients and healthy controls

3.2.1. Recruitment, sample collection and preparation

Patients previously diagnosed with TBDs and seen at the Ribeirão Preto Blood Center, FMRP-USP, were invited to join the study in case they met the inclusion criteria: short telomere length and/or presence of pathogenic variants in telomere-related genes identified by next-generation sequencing (NGS) or Sanger sequencing, and clinical manifestations related to TBDs, such as BMF, pulmonary fibrosis, liver fibrosis or cirrhosis, of both sexes and with ages ranging from 12 to 90 years old. Patients who had been submitted to bone marrow transplantation were not eligible. At the end, twenty patients joined the study. Clinical data was extracted from their existing medical records. Additionally, ten healthy subjects from the Ribeirão Preto area, of both sexes and with ages from 12 to 90 years old, with no history of familiar bone marrow failure, pulmonary or hepatic fibrosis, were recruited as controls. The study

was approved by the local Ethics Committee (CAAE: 28197220.6.0000.544; Attachment B) and conducted in accordance with the ethical standards as laid down in the Declaration of Helsinki.

Peripheral blood was collected in tubes containing EDTA or clot activator (silica), to obtain peripheral blood mononuclear cells (PBMCs) and serum, respectively. PBMCs were separated from whole blood by density gradient over Histopaque 1077 (Sigma-Aldrich), and aliquoted for DNA extraction and immunophenotyping, the latter being frozen in FBS with 10% DMSO at -80 °C until analysis. Genomic DNA was extracted with DNeasy Blood and Tissue kit (Qiagen, Maryland, USA), quantified, diluted to 50 ng/µL and stored at -20 °C. Serum was aliquoted and frozen at -80 °C until analysis.

3.2.2. Telomere length measurement

TL was determined by Southern Blot analysis of terminal restriction fragment (TRF), according to the manufacturer's instructions with minor changes (GUTIERREZ-RODRIGUES et al., 2014) (TeloTAGGG telomere Length Assay, #12209136001, Roche Applied Science, Mannheim, Germany). Genomic DNA (800 ng) was digested by restriction enzymes (*HinfI* and *RsaI*) at 37 °C, for 2 h. DNA fragments were then separated by electrophoresis in 0.8% agarose gel for 5 h. Gel was denatured and neutralized, and later transferred to a nylon membrane by Southern blotting, probed and detected by chemiluminescence. Mean TRF length was determined according to the formula TRF = Σ(ODi)/ Σ(ODi/Li), where ODi is the chemiluminescent signal and Li is the length of the fragment at a given position. The mean TRF of a known reference sample was included in every experiment to validate the results.

3.2.3. Mass cytometry (CyTOF)

For immunophenotyping, PBMCs were thawed in RPMI-1640 media containing 10% FBS, 1% Penicillin/Streptomycin and 1 µL/mL benzonase, washed and resuspended in complete media for counting. 5×10^6 cells per sample were transferred to V-bottom wells in a 96-well deep-well plate. Each sample was stained with a combination of three metal-tagged B2M antibodies for barcoding, and up to 20 samples were pooled in a single 5 mL tube. On total, 6 different metal isotopes were used to

tag B2M for barcoding combinations. Due to the limit of barcode combinations, samples were processed in two batches, and batch-control samples were used to control for batch variations. Cells were then washed and resuspended in Maxpar® Cell Staining Buffer (CSB). A total of 30×10^6 cells was taken and transferred to a new tube, and stained for surface and intracellular markers. Thirty-nine markers of cell lineages or state were used, and the full list of antibodies, clones and channels/metals are described in Chart 2. Cell viability was determined using 103Rh and 193Ir. After fixation with PFA, cells were passed through filter, counted, separated into multiple FACS tubes to a concentration of 0.5×10^6 cells/mL and loaded into a CyTOF XT™ equipment (Standard BioTools, Inc) for data acquisition. FCS files were concatenated into a single file for data processing and analysis.

Chart 2. List of antibodies used for mass cytometry.

Channel / Metal isotope	Antigen	Clone	Std. BioTools Cat. No.	Biolegend Cat. No.	BD Biosciences Cat. No.	Antibodies.com Cat. No.
114 Cd	B2M	2M2	NA	316302	NA	NA
116 Cd	B2M	2M2	NA	316302	NA	NA
194 Pt	B2M	2M2	NA	316302	NA	NA
195 Pt	B2M	2M2	NA	316302	NA	NA
196 Pt	B2M	2M2	NA	316302	NA	NA
198 Pt	B2M	2M2	NA	316302	NA	NA
89 Y	CD45	HI30	3089003B	NA	NA	NA
106 Cd	Vδ2	B6	NA	331402	NA	NA
110 Cd	CD3	UCHT1	NA	300438	NA	NA
111 Cd	CD4	RPA-T4	NA	300570	NA	NA
112 Cd	CD56	NCAM16.2	NA	NA	559043	NA
113 Cd	CD8	RPA-T8	NA	301002	NA	NA
141 Pr	CD196 (CCR6)	11A9	3141014A	NA	NA	NA
142 Nd	CD7	CD7-6B7	NA	343111	NA	NA
143 Nd	GZMB	CLB-GB11	NA	NA	NA	A86653
144 Nd	CD38	HIT2	3144014B	NA	NA	NA
145 Nd	IgD	IA6-2	NA	348235	NA	NA
146 Nd	CXCR5	J252D4	NA	356902	NA	NA
147 Sm	CD28	CD28.2	NA	302937	NA	NA
148 Nd	CD16	3G8	3148004B	NA	NA	NA
149 Sm	CD194 (CCR4)	L291H4	3149029A	NA	NA	NA
150 Nd	CD39	A1	NA	328202	NA	NA
151 Eu	CD103	Ber-ACT8	3151011B	NA	NA	NA
152 Sm	CD31	WM59	NA	303102	NA	NA
153 Eu	Vα7.2	3C10	3153024B	NA	NA	NA
154 Sm	CD161	HP-3G10	NA	339902	NA	NA

Continues

Chart 2 (continuation)

Channel / Metal isotope	Antigen	Clone	Std. BioTools Cat. No.	Biolegend Cat. No.	BD Biosciences Cat. No.	Antibodies.com Cat. No.
155 Gd	CD27	L128	3155001B	NA	NA	NA
158 Gd	CD183 (CXCR3)	G025H7	NA	353733	NA	NA
159 Tb	CD197 (CCR7)	G043H7	3159003A	NA	NA	NA
160 Gd	CD14	M5E2	NA	301843	NA	NA
161 Dy	CD152 (CTLA-4)	14D3	3161004B	NA	NA	NA
162 Dy	CD141	M80	NA	344102	NA	NA
163 Dy	CD1c	L161	NA	331502	NA	NA
164 Dy	CD95 (Fas)	DX2	3164008B	NA	NA	NA
165 Ho	CD127 (IL-7Ra)	A019D5	3165008B	NA	NA	NA
166 Er	CD25 (IL-2R)	M-A251	NA	356102	NA	NA
167 Er	TIGIT	A15153G	NA	372702	NA	NA
168 Er	Ki67	Ki-67	NA	350523	NA	NA
169 Tm	CD45RA	HI100	3169008B	NA	NA	NA
170 Er	T-bet	4B10	NA	644825	NA	NA
171 Yb	FoxP3	150D	NA	320002	NA	NA
172 Yb	CD19	HIB19	NA	302247	NA	NA
173 Yb	HLA-DR	L243	3173005B	NA	NA	NA
175 Lu	CD279 (PD-1)	EH12.2H7	3175008B	NA	NA	NA
176 Yb	CD123	6H6	NA	306027	NA	NA

3.2.4. Mass cytometry data processing, automated clustering, dimensionality reduction and visualization

Single, live cells were gated and debarcoding of samples was performed using FlowJo™ v.10.9.0 software (BD Biosciences). We next gated cells based on CD45 and CD3 expression, in order to generate FCS files for $CD45^+CD3^-$ and $CD45^+CD3^+$ cells for each individual sample. Each file was then used for automated clustering by self-organizing maps (Flow-SOM) (QUINTELIER et al., 2021)using the web-based software Cytobank (Cytobank, Inc). We first generated 20 metaclusters for $CD3^-$ cells and other 20 for $CD3^+$ cells and, following the identification of each population based on their markers, we excluded unspecific clusters and combined clusters with close similarity. Next step was dimensionality reduction and visualization, which was conducted using viSNE maps (AMIR et al., 2013) in Cytobank. Finally, the following major populations were manually gated using FlowJo: $CD4^+$ and $CD8^+$ T cells, B cells, T helpers (T_H) 1, 2, 17 and 17.1, recent thymic emigrants (RTE), $CD4^+CD95^+PD\text{-}1^+$, $CD8^+CD95^+PD\text{-}1^+$ and $C19^+CD95^+$ cells.

3.2.5. Flow cytometry for MAIT cells

Additional flow cytometry analysis was required for MAIT cells. For that, the following antibodies were used: anti-CD45 APC-H7 (#560274), anti-CD3 PE (#555333; BD Pharmigen), anti-CD161 Brilliant Violet 510™ (#339922; Biolegend), anti-TCR Vα7.2 Brilliant Violet 421™ (#351716; Biolegend), anti-CD38 PE Cy7 (#335790; BD Pharmigen), anti-HLA-DR FITC (#347400) and 7-AAD (#559925; BD Pharmigen). Data was analyzed using FlowJo v.10.9.0 software (BD Biosciences), and MAIT cells were defined as $CD45^+CD3^+CD161^{hi}V\alpha7.2^+$.

3.2.6. Measurement of serum cytokines, chemokines and growth factors

We designed a panel to assess the serum levels of 32 analytes by Luminex™ xMAP™ technology (Chart 3), in a MAGPIX™ instrument (Luminex, Austin, TX, USA) (Table 4). The panel was manufactured by ThermoFisher and the web-based software ProcartaPlex™ Analysis App (ThermoFisher) was used for data analysis.

Additionally, TGF-β1 was determined by conventional enzyme-linked immunosorbent assay (ELISA), using the TGF-β1 Pre-Coated Human ELISA kit (#BGK01137; Peprotech).

Chart 3. Luminex™ panel for cytokines, chemokines and growth factors.

Luminex™ 32-plex assay panel		
Angiopoietin-1	IL-16	IL-7
Eotaxin	IL-18	IL-8
FGF-2	IL-1RA	MCP-1
HGF	IL-2	M-CSF
IFN-α	IL-22	MIP-1 α
IFN-γ	IL-23	MIP-3 α
IL-17A	IL-27	MMP-1
IL-1 alpha	IL-3	PDGF-BB
IL-1 beta	IL-4	TNF-α
IL-10	IL-5	VEGF-A
IL-15	IL-6	

3.2.7. Quantification of TRECs and KRECs in peripheral blood

Peripheral blood was collected on Guthrie cards, and a 3.2 mm dried blood spot punch was used for T-cell excision circle (TREC) and kappa-deleting recombinant excision circle (KREC) analysis by qPCR, as described elsewhere (BORTE et al., 2012; KANEGAE et al., 2017).

3.2.8. Statistical analysis

The frequencies of each Flow-SOM-generated metacluster were compared by Mann-Whitney *U* test. Manually gated populations were compared by Mann-Whitney or unpaired Student's *t* test (with Welch's correction when applicable), depending on their normality, assessed by Shapiro-Wilk test. Cytokines, chemokines and growth factors presented highly skewed distribution across samples; therefore, logarithmic transformation was used. In this case, geometric means with interquartile ranges (Q1-Q3) are presented as better measures of central tendency and dispersion than arithmetic means and standard deviations (SD). Due to the small sample size, the presence of outliers and possible deviations from normality, bootstrap t-tests were used to compare between means of two groups (or geometric means) (EFRON &

TIBSHIRANI, 1993). The “boot.t.test” function of the CRAN “MKinfer” package, available in R software, was used to obtain the bootstrapped *p*-values. In situations where three groups are compared, a bootstrap test based on the Welch-James statistic and trimmed means was used (WILCOX, 1997; KESELMAN et al., 2003). Corresponding *p*-values were obtained using the “welchADF.test” function of the CRAN “welchADF” package of the R software (VILLACORTA, 2017). Spearman's correlation coefficient was used to analyze associations between TL z-scores and the variables of interest. TL z-scores were calculated based on the TL from 301 healthy donors, present on a database from our group. All *p*-values were corrected by Benjamini-Hochberg false-discovery rate (FDR), and values ≤0.05 were considered significant. The R software version 4.1.1 and GraphPad Prism v.9.5.1 (GraphPad Software, Boston, Massachusetts, USA) were used to analyze the data.

4. RESULTS

4.1. Murine model

4.1.1. Telomere length and induction of liver fibrosis

Measurement of TL showed that both knockout groups presented lower T/S in leukocytes and liver, indicating that the absence of *Terc* or *Tert* is sufficient to drive telomeric shortening in mice (Figures 3A and 3B). WT animals had a mean leukocyte T/S of 0.99±0.30, while *Terc*$^{-/-}$ and *Tert*$^{-/-}$ presented a mean of 0.45±0.14 and 0.69±0.22, respectively (p<0.0001). For liver samples, mean T/S was of 1.0±0.21 for WT, 0.67±0.16 for *Terc*$^{-/-}$ and 0.87±0.27 for *Tert*$^{-/-}$ (p<0.0001). For both analysis, *Terc*$^{-/-}$ mice significantly lower TL when compared to WT and *Tert*$^{-/-}$. Moreover, TL in leukocytes and liver tissue significantly correlated to each other (Figure 3C).

Figure 3. Telomere length in leukocytes and liver tissue of mice.

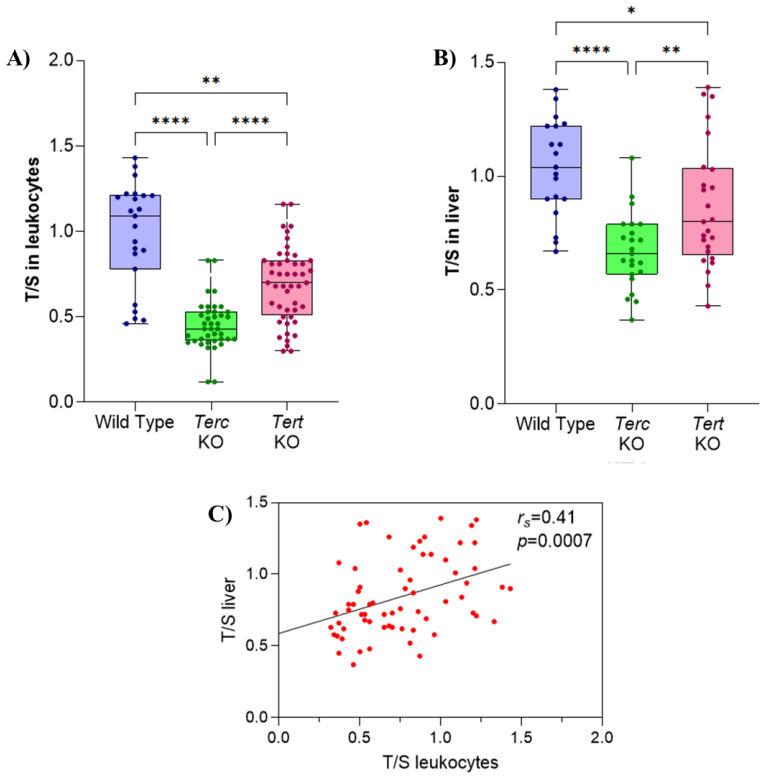

Telomere length in mice was measured by qPCR, from DNA extracted from blood and liver sections. **(A)** T/S ratio in leukocytes. **(B)** T/S ratio in liver fragments. **(C)** Spearman correlation between leukocytes and liver T/S ratios. $^{*}p \leq 0.05$; $^{**}p \leq 0.01$; $^{****}p \leq 0.0001$.

Following 45 days post-inoculation, *S. mansoni* eggs began to appear in stool samples from infected mice (Figure 4A), which is in accordance to what has been previously described (CHEEVER *et al.*, 2002). Animals were euthanized with an overdose of ketamine/xylazine after 12 weeks post-infection and, during necropsy, it was observed that infected mice presented with hepatosplenomegaly, and their liver had a dark coloration with multiple inflammatory foci, as shown in Figure 4B.

Figure 4. Induction of liver fibrosis by infection with *S. mansoni*

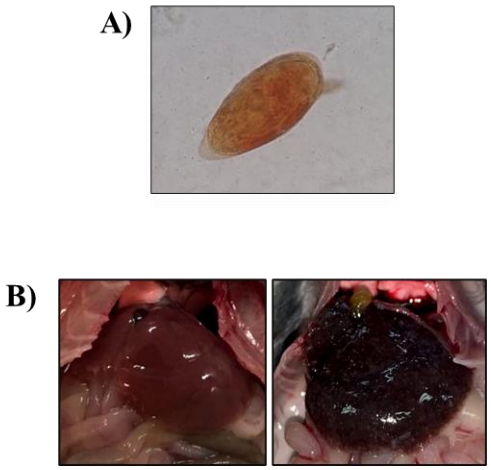

Infection of mice with *S. mansoni* leads to hepatic enlargement and inflammation. **(A)** *S. mansoni* egg found in stool samples from infected mice. **(B)** Liver samples from healthy (left) and infected (right) mice.

Body mass was reduced in WT and *Tert*$^{-/-}$ infected mice (21±4.8 g; 20±3.0 g; respectively), when compared to their non-infected counterparts (24±3.2 g; 22±3.1 g; respectively, $p<0.05$). For *Terc*$^{-/-}$ animals, no significant mass reduction was observed in infected mice, however, it is worth noting that non-infected *Terc*$^{-/-}$ animals had lower mass when compared to non-infected WT mice ($p=0.0006$; Figure 5A). Organ masses were assessed and relative mass was calculated, based on body mass. All groups presented hepatomegaly when infected with *S. mansoni,* but *Terc*$^{-/-}$ mice had a less pronounced increase in liver mass ($p=0.0005$; Figure 5B). A similar result was found for spleen masses, with all three groups presenting enlarged spleen when infected, and *Terc*$^{-/-}$ animals having lower values when compared to *Tert*$^{-/-}$ ($p=0.007$; Figure 5C).

Figure 5. Body mass, liver and spleen relative masses in mice.

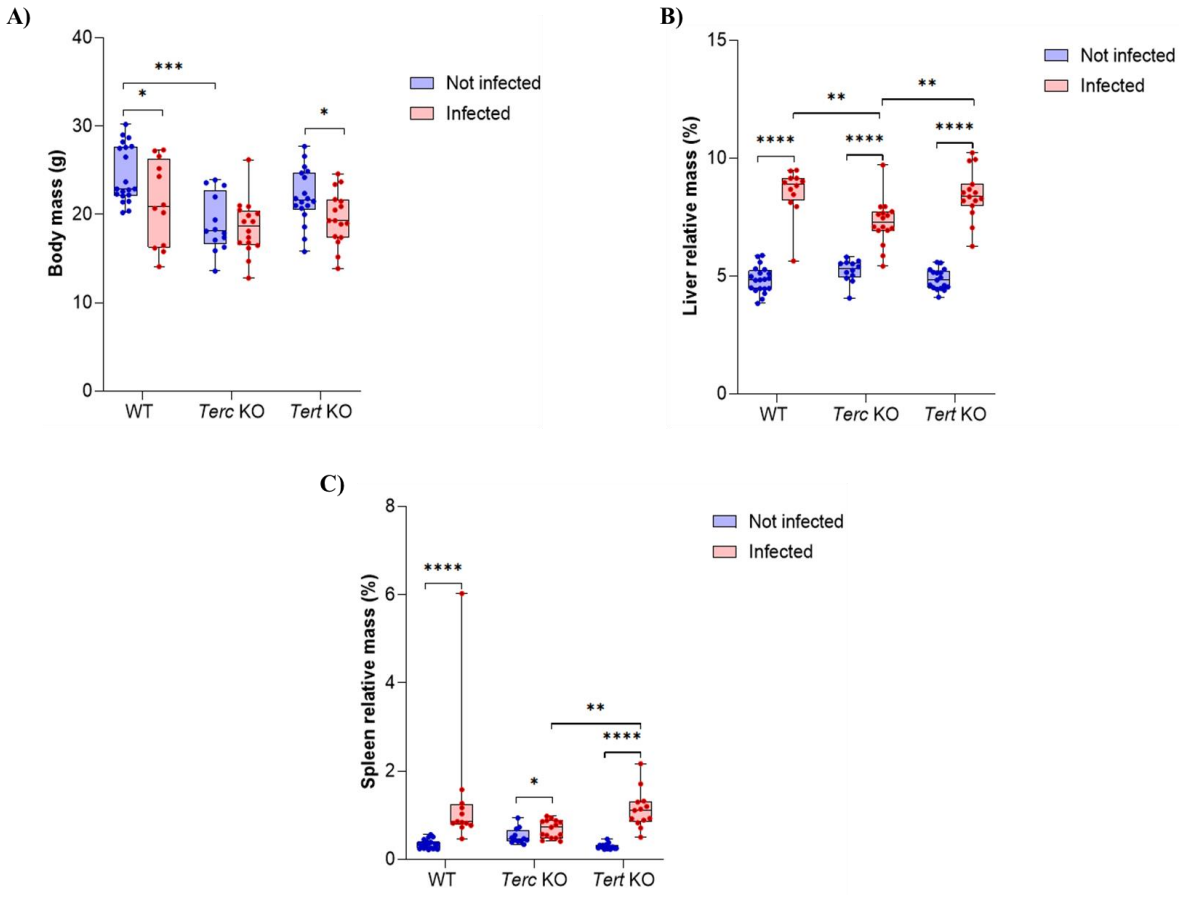

Following infection with *S. mansoni,* mice present alterations in body and organ masses. **(A)** Body mass after 12 weeks post-infection. **(B)** Liver relative mass, based on body mass. **(C)** Spleen relative mass, based on body mass. $^{*}p \leq 0.05$; $^{**}p \leq 0.01$; $^{***}p \leq 0.001$; $^{****}p \leq 0.0001$.

4.1.2. Histopathological evaluation of liver fibrosis

Liver tissue was first stained with HE, and large granulomas were observed around *S. mansoni* eggs trapped within the tissue of all groups (Figure 6A). Liver fibrosis index was assessed by staining with Picro-Sirius Red, which gives a reddish color to collagen fibers present in the tissue. In non-infected mice, collagen staining was minimal, being predominantly observed in arteries and not within liver parenchyma. Large fibrotic areas were visible in infected livers, especially in WT mice (Figure 6B).

Figure 6. Histopathological analysis of the liver of infected and non-infected mice.

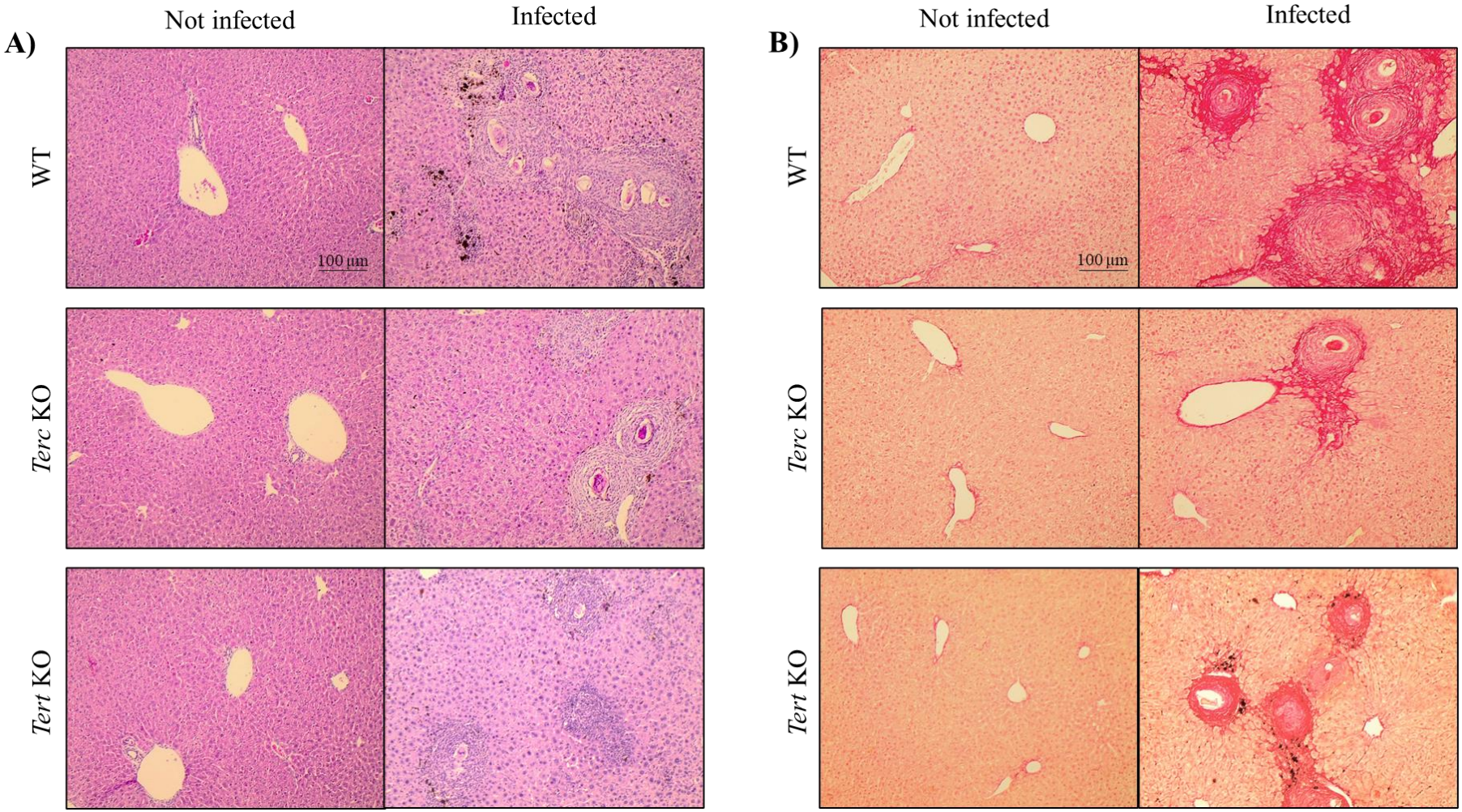

Histopathological analysis shows the presence of granulomas and collagen deposition in livers from mice infected with *S. mansoni.* **(A)** HE staining of liver tissue, 400× magnification. **(B)** Picro-Sirius Red staining of liver tissue, evidencing fibrotic areas in infected mice, 400× magnification.

Infected WT mice presented a mean fibrotic area of 13±4.2%, while *Terc*$^{-/-}$ presented 7.2±4.3% and *Tert*$^{-/-}$ 9.3±5.1%. The difference between WT and *Terc*$^{-/-}$ animals was statistically significant (p=0.004), which shows that the knockout animals had less fibrotic lesions. Although the same was not significant for *Tert*$^{-/-}$, the mean index was also lower in such group (p=0.09). Figure 7 shows all comparisons among groups.

Figure 7. Liver fibrosis index in infected and non-infected mice.

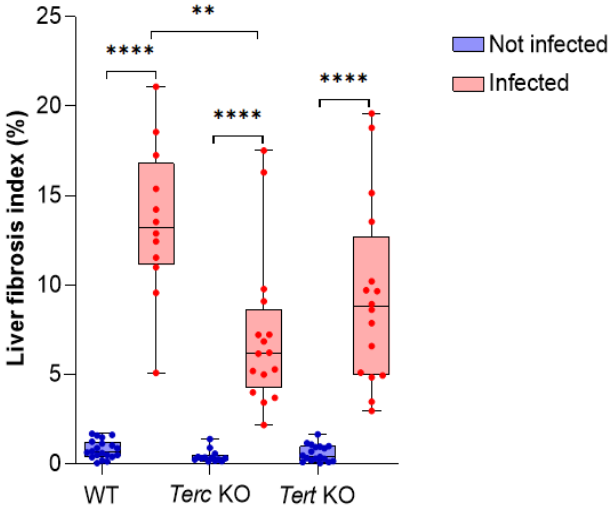

Liver fibrotic index, based on Picro-Sirius Red staining of collagen fibers. $^{**}p\leq0.01$; $^{****}p\leq0.0001$.

4.1.3. Immunohistochemistry for macrophage staining

Immunohistochemistry (IHC) was applied for the identification of macrophages infiltrated within granulomas in the liver tissue of infected mice. For that, F4/80, CD68, iNOS and CD206 markers were employed. Figure 8 depicts representative sections stained with F4/80, iNOS and CD206, in all different groups, while Figures 9A-D shows mean frequencies of each marker.

Figure 8. Immunohistochemical staining of macrophages in liver sections.

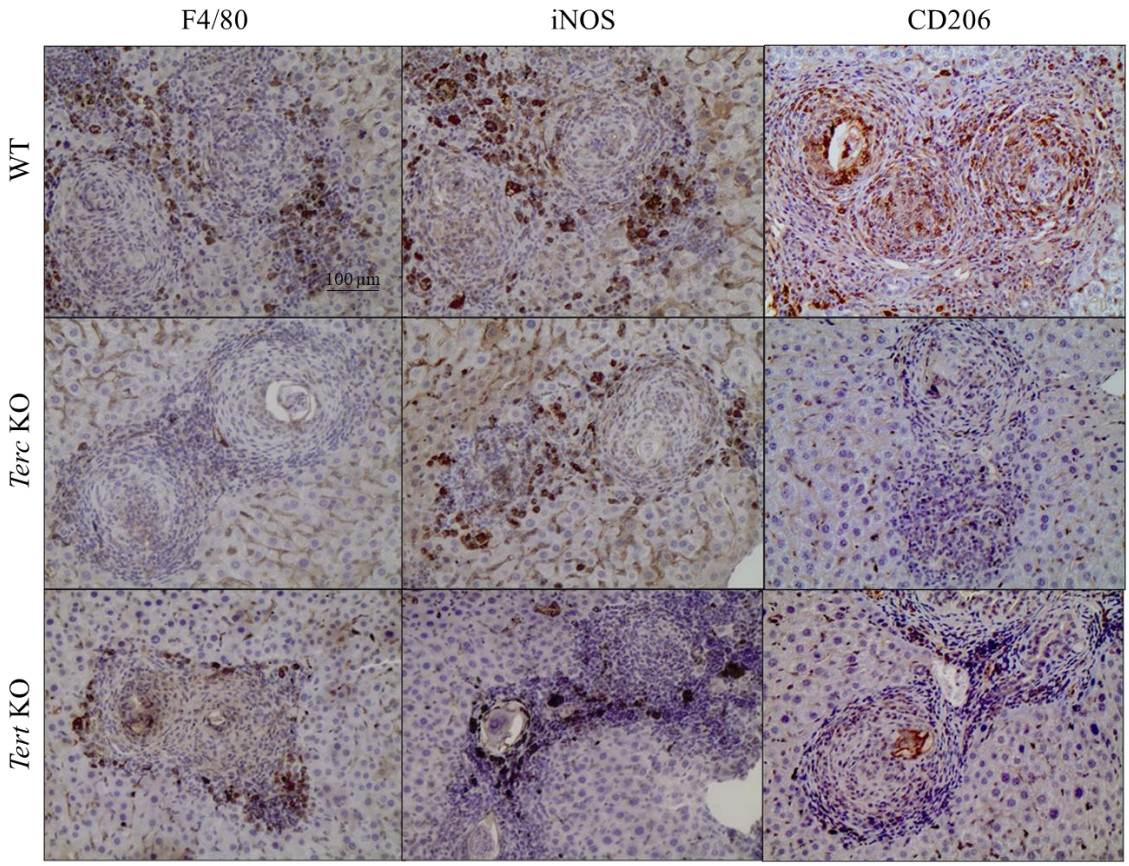

Immunohistochemistry staining of liver sections from mice infected with *S. mansoni.*

Pan-macrophage marker, F4/80, was found in a higher frequency in WT animals (23±10%) when compared to *Terc*$^{-/-}$ (5.2±8.1%; $p<0.0001$) and *Tert*$^{-/-}$ (12±8.2%; $p=0.03$). The same pattern was observed for iNOS and CD206, while for CD68, a significant difference was seen between WT and *Terc*$^{-/-}$ mice. For all markers, frequencies were lower in *Terc*$^{-/-}$ animals, which prompted us to look for correlations with fibrosis index. F4/80 and iNOS were positively correlated with liver fibrosis index ($r_S=0.41$, $p=0.006$; $r_S=0.53$, $p=0.0002$; respectively). No significant correlations were observed for CD68 and CD206 (Figures 9E-H).

Figure 9. Frequencies of F4/80, iNOS, CD68 and CD206 in liver samples, and correlation with liver fibrosis index.

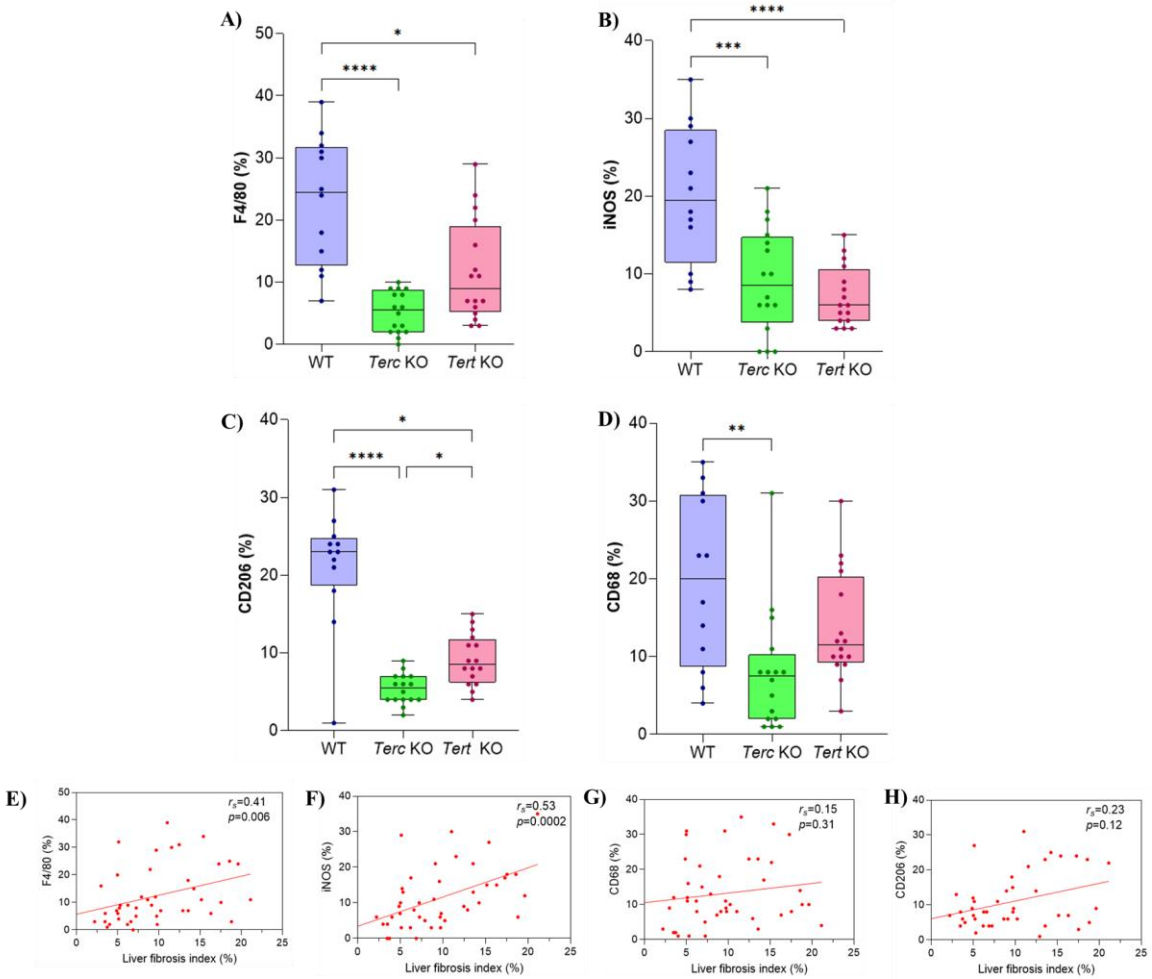

Macrophage infiltration occurs during granuloma formation and cells can be detected by IHC staining. Percentage of positive cells for **(A)** F4/80, **(B)** iNOS, **(C)** CD206 and **(D)** CD68. **(E-H)** Correlations with liver fibrosis index. $^{*}p \leq 0.05$; $^{**}p \leq 0.01$; $^{***}p \leq 0.001$; $^{****}p \leq 0.0001$.

4.1.4. In vitro polarization of bone marrow-derived macrophages

After 7 days of culture, BMDMs were collected for gene expression analysis and supernatant was used for nitrite measurement in LPS stimulated cells. Nitrite quantification (Figure 10A), determined by Griess method, did not show significant differences between groups, although *Tert*$^{-/-}$ mice had a lower mean concentration (17±1.5 µM/10^6 cells; *Terc*$^{-/-}$ = 22±2.8 µM/10^6 cells; WT = 22±5.2 µM/10^6 cells). Nonetheless, the expression of genes associated to classical activation of macrophages (M1) was significantly different among groups, with knockout BMDMs showing reduced capacity of polarization following LPS treatment (Figures 10B-D).

Emphasis should be given to *Tnf-α,* as it was the less expressed gene in *Terc*$^{-/-}$ and *Tert*$^{-/-}$ BMDMs following LPS stimulus.

On the other hand, stimulation with IL-4 promoted the expression of *Arg1* and *Cd206* in all groups of BMDMs, and telomerase-knockout cells had an even stronger expression of such genes, when compared to WT cells (Figures 10E-F).

Figure 10. In vitro polarization of bone marrow-derived macrophages

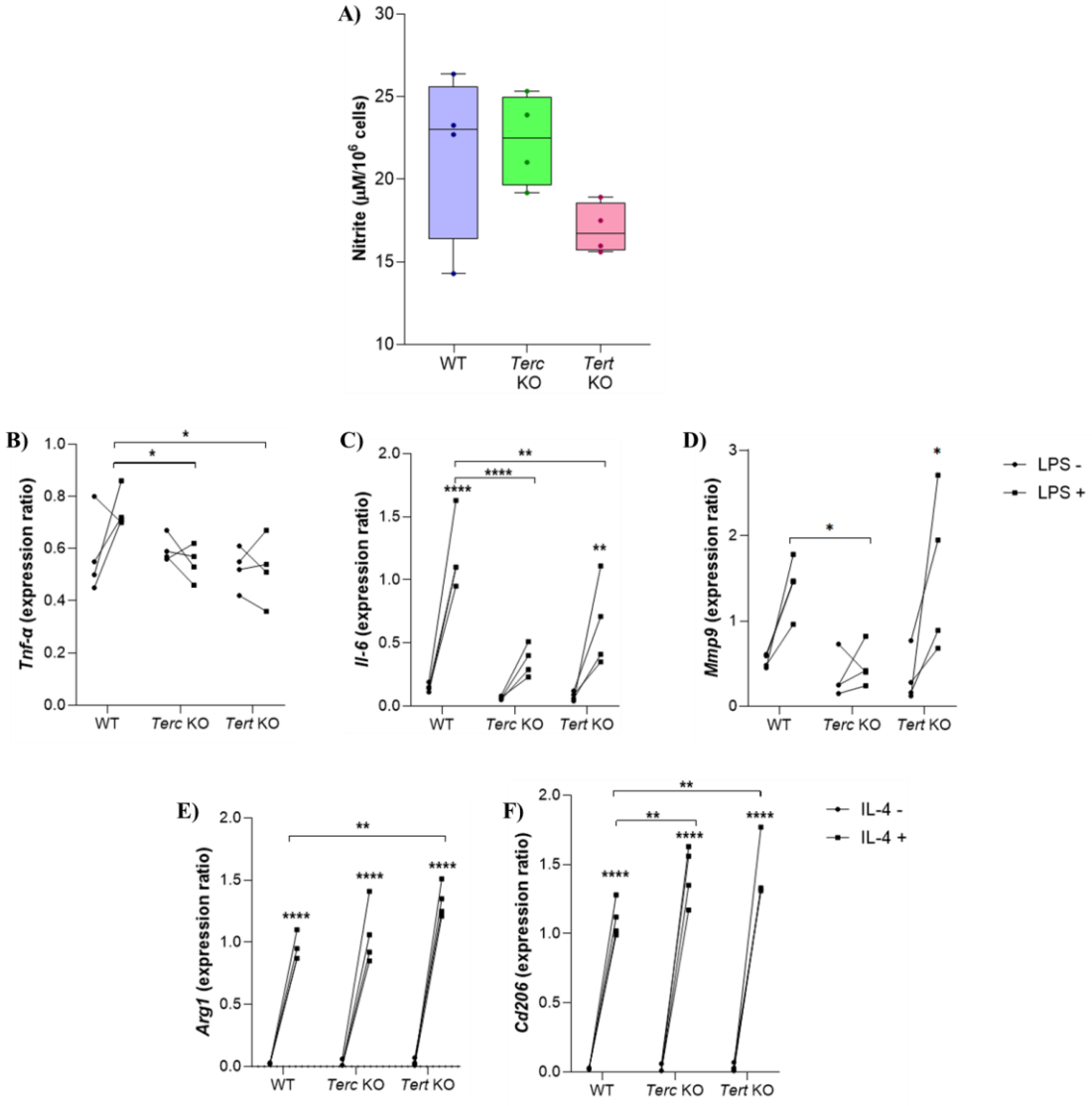

BMDMs are cultured for 7 days and then stimulated with either LPS or IL-4. **(A)** Nitrite quantification by Griess method in LPS-treated supernatant. **(B-D)** Expression of genes activated during classical polarization of BMDMs with LPS. **(E** and **F)** Expression of genes activated during alternative polarization of BMDMs with IL-4. $^{*}p\leq0.05$; $^{**}p\leq0.01$; $^{****}p\leq0.0001$.

4.1.5. Measurement of plasmatic cytokines

Plasma samples from infected mice were used for the measurement of the following cytokines: IFN-γ, TNF-α, IL-2, IL-4, IL-6, IL-10 and IL-17A. Results are shown in Figure 11. No significant differences were observed for IFN-γ, TNF-α, IL-2, IL-6 and IL-10 (p>0.05). IL-4 and IL-17A, however, were reduced in samples from *Terc-/-* mice, which is likely to be related to the lowest level of fibrosis observed in this group.

Figure 11. Plasmatic levels of cytokines in mice.

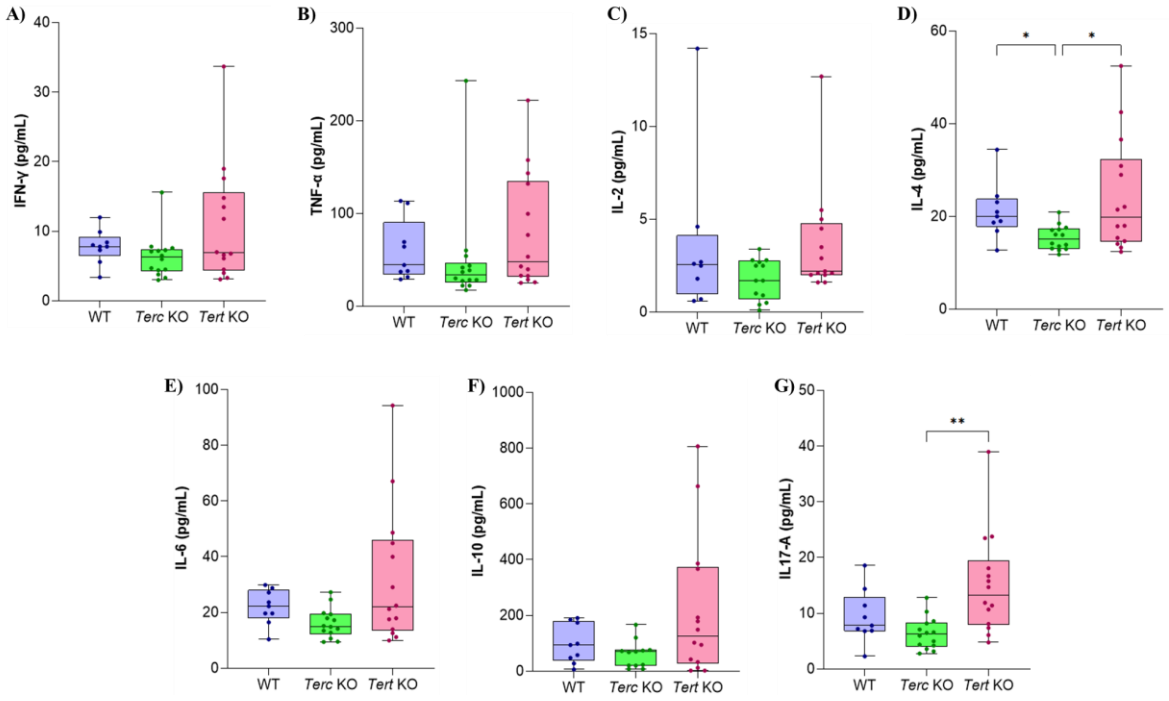

Measurement of plasmatic cytokines by CBA, in mice. **(A-G)** Levels of cytokines in plasma of *S. mansoni* infected mice. $^{*}p\leq0.05$; $^{**}p\leq0.01$.

To test whether the cytokines levels were associated with the levels of fibrosis, we applied Spearman correlations tests. All seven analytes were positively correlated to fibrosis index, as shown in Table 2.

Table 2. Spearman correlation between cytokines and liver fibrosis index.

Cytokine	Spearman r_s	*P*-value
IFN-γ	0.43	0.0082**
TNF-α	0.36	0.031*
IL-2	0.35	0.041*
IL-4	0.52	0.0010***
IL-6	0.52	0.0009***
IL-10	0.46	0.0054**
IL-17A	0.36	0.029*

4.2. TBD patients and healthy controls

4.2.1. Volunteers' characteristics and Flow-SOM automated clustering of CyTOF data

Table 3 describes the characteristics of patients and healthy individuals included in the study. Eighteen patients (90%) had a TL below the 10th percentile (short), with eight of them falling below the 1st percentile (very short). Two patients (10%), had normal TL, despite having pathogenic variants identified in *TERT* and *RTEL1*; both, however, presented TBD-related clinical manifestations, including liver disease with portal hypertension and lung diseases, and the patient harboring a variant in *RTEL1* also had BMF. All healthy individuals had normal age-adjusted TL, falling between the 20th and 95th percentile (Table 3; Figure 12). Liver and/or lung disease was present in 60% of patients, and all clinical manifestations are shown in Table 4.

Table 3. General characteristics of TBD patients and healthy controls included in the study.

Sample code	Group	Age (years)	Sex	Expected TRF[c] (kb[d])	Observed TRF (kb)	TL[e] percentile	TL z-score[f]
T342	Patient	13.6	M[a]	8.5	3	< 1st	-3.83
T86	Patient	33.6	M	7.3	2.8	< 1st	-3.14
T801	Patient	26.0	F[b]	7.5	3.3	< 1st	-2.93
T1009	Patient	37.7	M	7	3.1	< 1st	-2.72
T693	Patient	20.8	F	7.9	4	< 1st	-2.72
T546	Patient	37.9	M	7.1	3.5	< 1st	-2.53
T548	Patient	31.6	F	7.2	3.7	< 1st	-2.44
T521	Patient	32.7	M	0.72	3.8	< 10th	-2.38
T420	Patient	12.8	M	8.6	5.3	< 10%	-2.31
T310	Patient	28.3	M	7.4	4.2	< 1st	-2.24
T881	Patient	56.9	F	6.7	3.6	< 10th	-2.17
T256	Patient	49.2	F	6.8	3.9	< 10th	-2.06
T324	Patient	30.1	F	7.3	4.4	< 10th	-2.06
T141	Patient	49.4	F	7	4.1	< 10th	-2.03
T924	Patient	62.5	F	6.7	4.6	< 10th	-1.48
T421	Patient	41.3	M	7.1	5.1	< 10th	-1.41
T664	Patient	34.2	M	7.3	5.4	< 10th	-1.34
T78	Patient	57.2	F	6.8	5.5	10-20th	-1.30
T127	Patient	55.7	F	6.7	5	< 10th	-1.20
T85	Patient	64.8	M	6.3	5.9	30-40th	-0.30
C1	Healthy	29.4	F	7.28	7.70	60-70th	0.27
C2	Healthy	35.7	F	7.06	7.30	50-60th	0.14
C3	Healthy	24.9	M	7.50	7.10	30-40th	-0.30
C4	Healthy	32.0	M	7.18	8.50	80-84th	0.89
C5	Healthy	13.9	M	8.34	8.00	40-50th	-0.26
C6	Healthy	35.4	F	7.10	9.10	90-95th	1.36
C7	Healthy	32.2	F	7.17	7.20	50-60th	0.00
C8	Healthy	52.7	F	6.77	7.00	50-60th	0.14
C9	Healthy	56.3	M	6.74	5.30	15-20th	-1.02
C10	Healthy	27.9	M	7.35	9.40	90-95th	1.40

[a]Male; [b]Female; [c]Terminal restriction fragment; [d]Kilobases; [e]Telomere length; [f]z-score calculated from 301 healthy subjects' samples from the group's database.

Figure 12. Telomere length in TBD patients and healthy controls

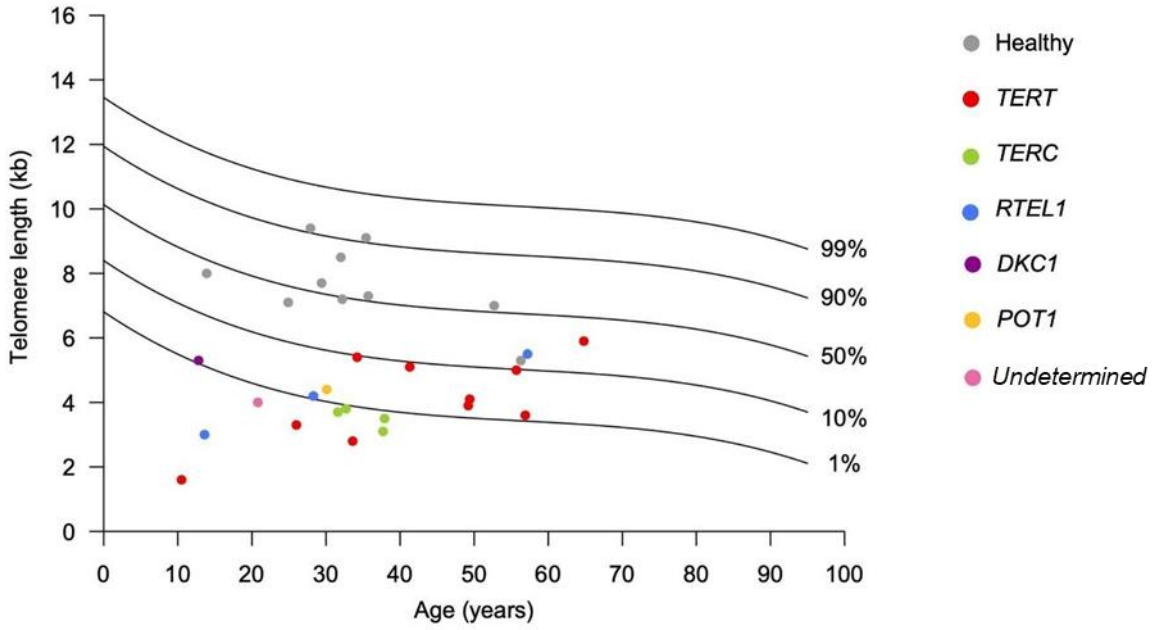

Telomere length (kilobases) of healthy controls and patients and their respective affected genes. <10th percentile = short; <1st percentile = very short.

Table 4. Variants and clinical manifestations presented by TBD patients included in the study.

Sample Code	Affected gene	Variant	Zygosity	BMF	Liver disease	Lung disease	Androgen
T342	*RTEL1*	c.A3257G p.Y1086C and c.3775_3776del p.A1259Lfs*2	het and het	Yes	No	No	Nandrolone
T86	*TERT*	c.G2594A p.R865H	het	Yes	No	No	-
T801	*TERT*	c.C1891T p.R631W	het	Yes	No	No	-
T1009	*TERC*	n.314_315del	het	Yes	Portal hypertension / Chronic hepatopathy	No	Danazol
T693	-	not detected	-	Yes	No	No	Danazol
T546	*TERC*	n.110_113delGACT	het	Yes	Steatosis	Small airway disease	Danazol
T548	*TERC*	n.110_113delGACT	het	Yes	No	No	-
T521	*TERC*	n.110_113delGACT	het	Yes	No	IPF	Danazol
T420	*DKC1*	c.C1058T p.A353V	hemi	Yes	No	No	-
T310	*RTEL1*	c.3775_3776del p.A1259Lfs*2	het	Yes	No	IPF	Danazol
T881	*TERT*	c.C193A p.P65T	homo	Yes	No	Pulmonary interstitial disease	-
T256	*TERT*	c.C193A p.P65T	homo	No	Chronic Hepatopathy	Small airway disease	-
T324	*POT1*	c.C437T p.P146L	het	Yes	No	N	-
T141	*TERT*	c.G2594A p.R865H	het	Yes	No	Small airway disease	-
T924	*TERT*	c.G2368A p.V790I	het	Yes	Portal hypertension / Chronic hepatopathy	IPF	-
T421	*TERT*	c.G2594A p.R865H	het	No	Steatosis	NO	-
T664	*TERT*	c.C3234G p.F1078L	het	No	No	Broncopathy	-
T78	*RTEL1*	c.C2227T p.R743X	het	Yes	Portal hypertension / Chronic hepatopathy	IPF	-
T127	*TERT*	c.C3234G p.F1078L	het	Yes	No	NO	-
T85	*TERT*	c.G2594A p.R865H	het	No	Portal hypertension / Chronic hepatopathy	Emphysema / Diffuse broncopathy	-

For CyTOF high-dimensional analysis, 20 clusters were initially created for each CD3 population, followed by merging of similar clusters or deletion of unspecific subsets, resulting in 14 clusters for $CD3^+$ and 15 for $CD3^-$ cells (Figure 13).

Figure 13. Metaclusters generated by Flow-SOM for $CD3^-$ and $CD3^+$ cells.

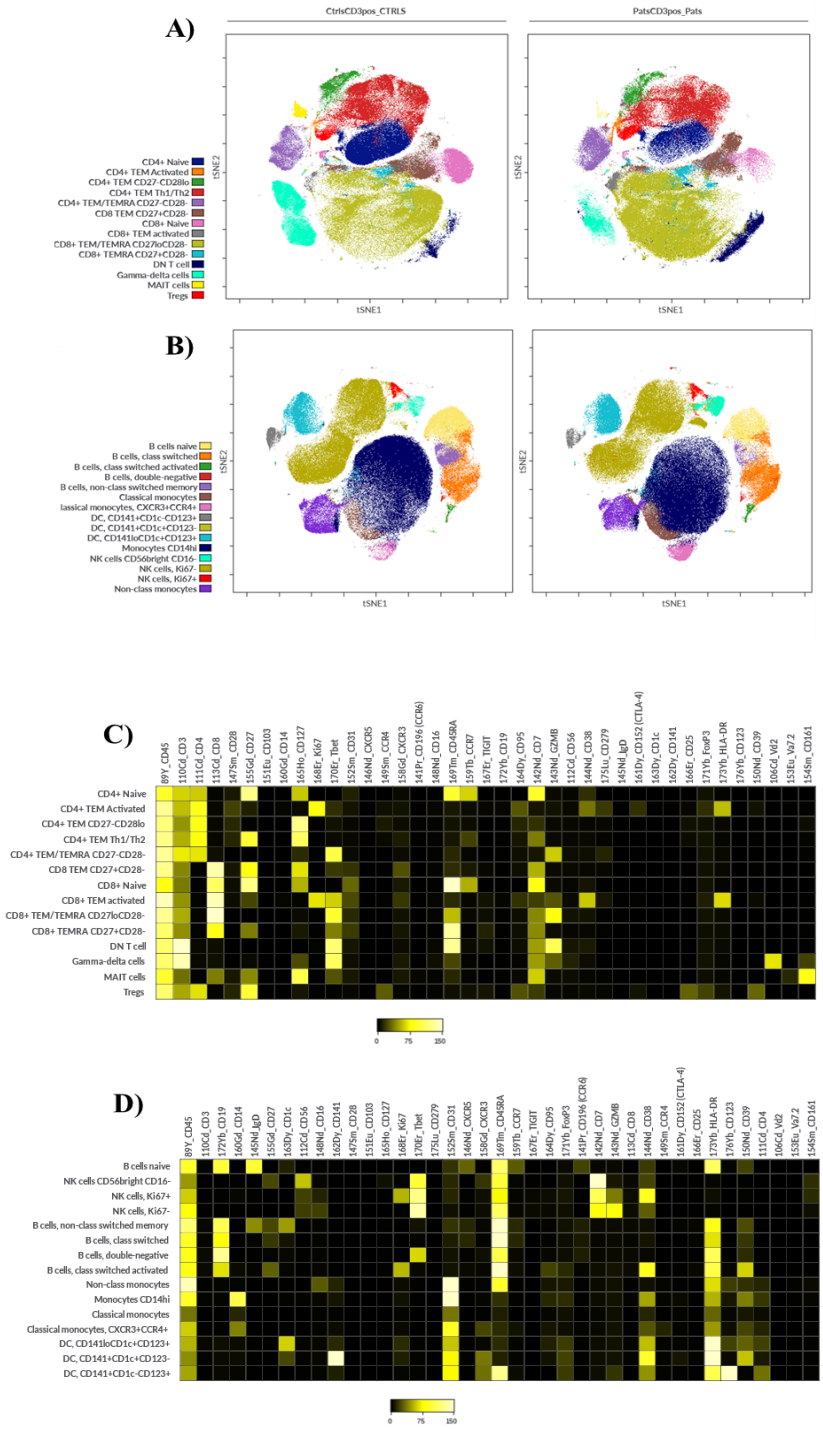

After initial gating for $CD3^+$ and $CD3^-$ cells, 14 subsets of $CD3^+$ cells were identified as shown in **(A)**, plus 15 subsets in $CD3^-$ as shown in **(B)**. **(C** and **D)** Metacluster heatmaps showing the relative expression of 39 markers amongst the identified clusters in $CD3^+$ and $CD3^-$ cells, respectively.

The identification of major populations on viSNE maps was based on pan-markers, and Figure 14 depicts the main subsets on $CD3^+$ cells, identified by CD4, CD8, Vα7.2 and Vδ2, while $CD3^-$ subsets are shown in Figure 15, and are identified by the expression of CD19, CD56, CD14, CD141 and CD1c.

Figure 14. Expression of main lineage markers in $CD3^+$ cells from patients and controls.

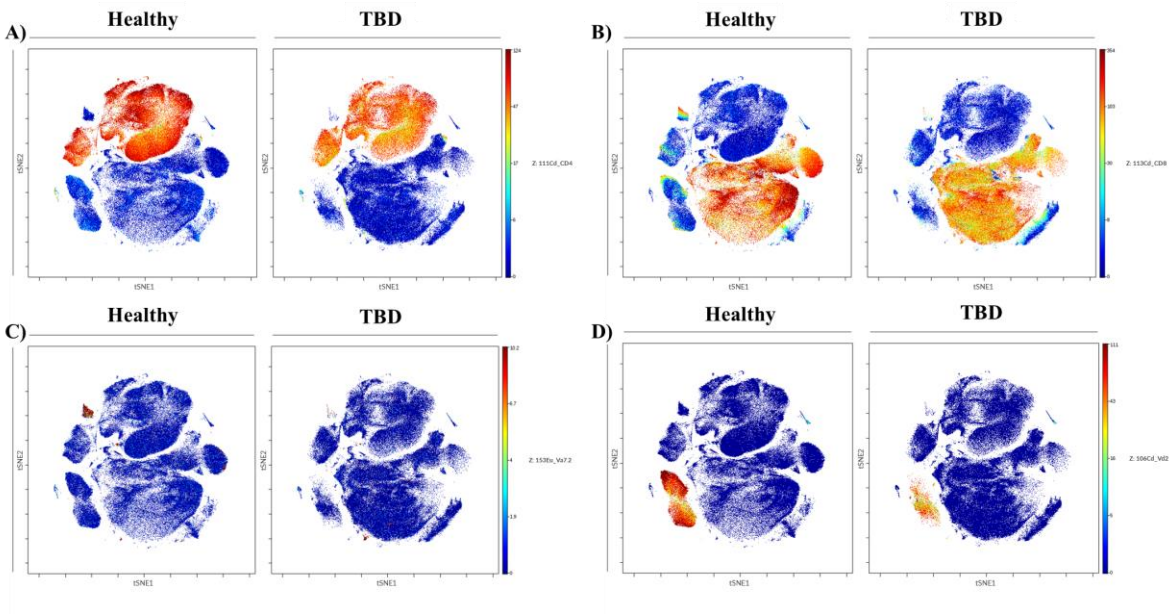

Channel colored viSNE maps showing the median of expression of the four main lineage markers for CD3+ cells. **(A)** Expression of CD4. **(B)** Expression of CD8. **(C)** Expression of TCR Vα7.2. **(D)** Expression of Vδ2.

Figure 15. Expression of main lineage markers in $CD3^-$ cells from patients and controls

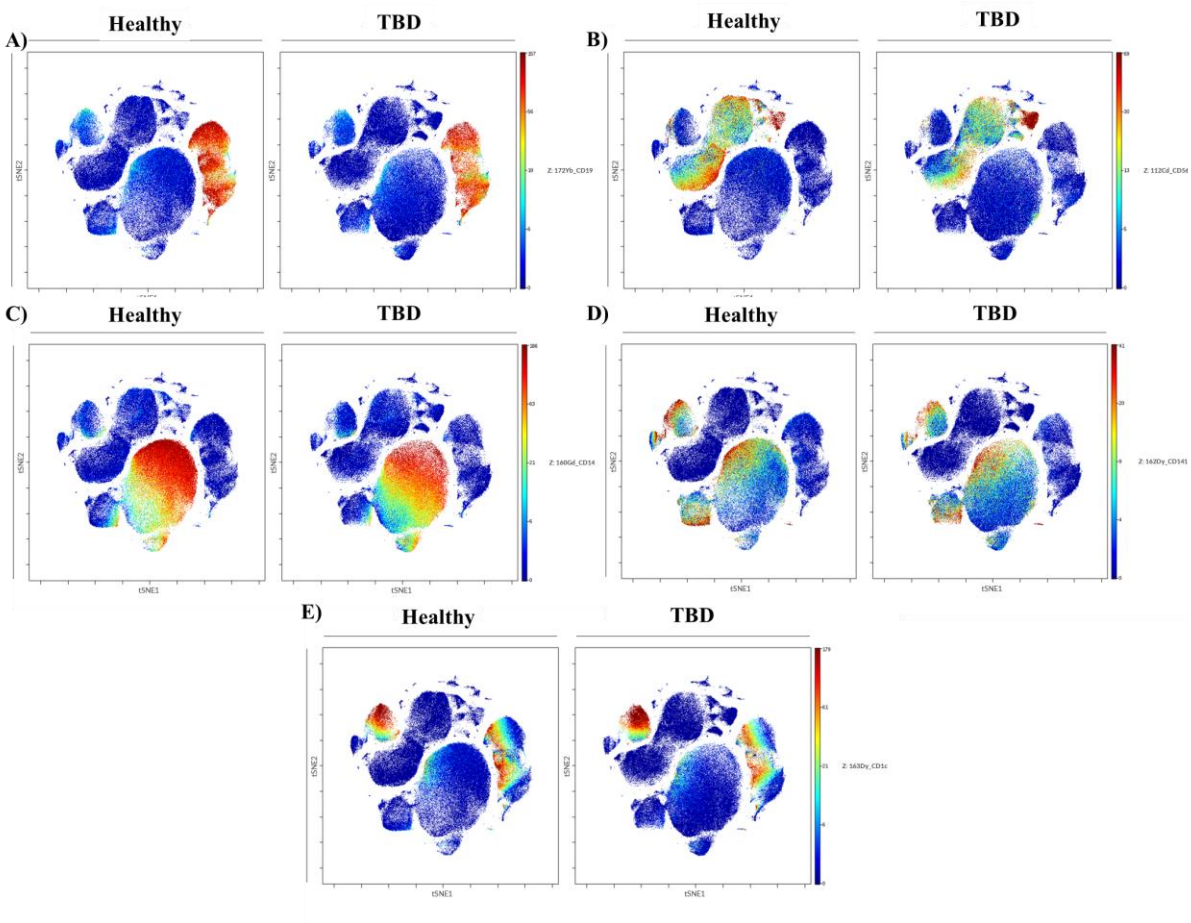

Channel colored viSNE maps showing the median of expression of the four main lineage markers for CD3- cells. **(A)** Expression of CD19. **(B)** Expression of CD56. **(C)** Expression of CD14. **(D)** Expression of CD141. **(E)** Expression of CD1c.

4.2.2. Phenotypical characteristics of lymphocytes

Short telomere syndromes notoriously recapitulate phenotypical manifestations acquired with aging (WAGNER *et al.*, 2018); thus, we expected to find immune alterations in our cohort typically observed in the elderly. TBD patients had lower frequency of $CD4^+$ T lymphocytes (33.0±13.7% of $CD3^+$ vs. 46.6±15.9% of $CD3^+$ in controls; p=0.049), whereas they exhibited an accumulation of $CD8^+$ T cells (53.9±14.4% of $CD3^+$ vs. 41.2±11.1% of $CD3^+$ in controls; p=0.043) (Figures 16A-B). CD4/CD8 ratio was lower than 1.0 in 80% of patients (Figure 16C). Patients also had fewer B cells (11.1±8.13% of $CD3^-$ vs. 17.5±7.23% of $CD3^-$ in controls; p=0.046) (Figure

16D). Naïve T ($CD45RA^+CCR7^+$) $CD4^+$ and $CD8^+$, and B ($CD19^+CD27^-IgD^+$) lymphocytes were markedly reduced in TBD, with low frequencies being observed for all three populations (Figures 16E-G) A subset of $CD8^+$ T effector memory/terminally differentiated effector memory (TEM/TEMRA) cells being $CD27^{lo}CD28^-$ was increased in patients (39.0±17.4% of $CD3^+$ vs. 20.5±12.5% of $CD3^+$ in controls; p=0.036) (Figure 16I). Regarding B cells, IgM or non-class switched memory B cells ($CD19^+CD27^+IgD^+$) were reduced in TBD (0.57±0.67% of $CD3^-$ vs. 2.64±1.79% of $CD3^-$ in controls; p=0.0074) (Figures 16H and J).

Because naïve T lymphocytes were reduced, we sought to explore the thymic output by looking for RTEs, defined as $CD31^+CD45RA^+$ cells. Decreased fractions were observed for both $CD4^+$ and $CD8^+$ subsets (Figure 17A), which is indicative of thymus hypofunction. To further scrutinize this hypothesis, we collected new samples from 10 patients and 10 age-matched controls, in order to quantify TRECs by qPCR. KRECs, indicative of B cell development, were also assessed. As a result, TREC copies were significantly low in TBD patients (Figure 17B), with 4 (40%) having undetectable copies of this biomarker. One pediatric patient (12.3 years old) presented only 1 TREC copy/µL of blood. Moreover, TRECs were inversely correlated with age in controls (r_S=-0.66, p=0.043), but not in patients (r_S=-0.25, p=0.48), as the premature shortening of telomeres is assumed to be sufficient to impair T cell development (Figures 17C-D).

Figure 16. Phenotypical characteristics of lymphocytes.

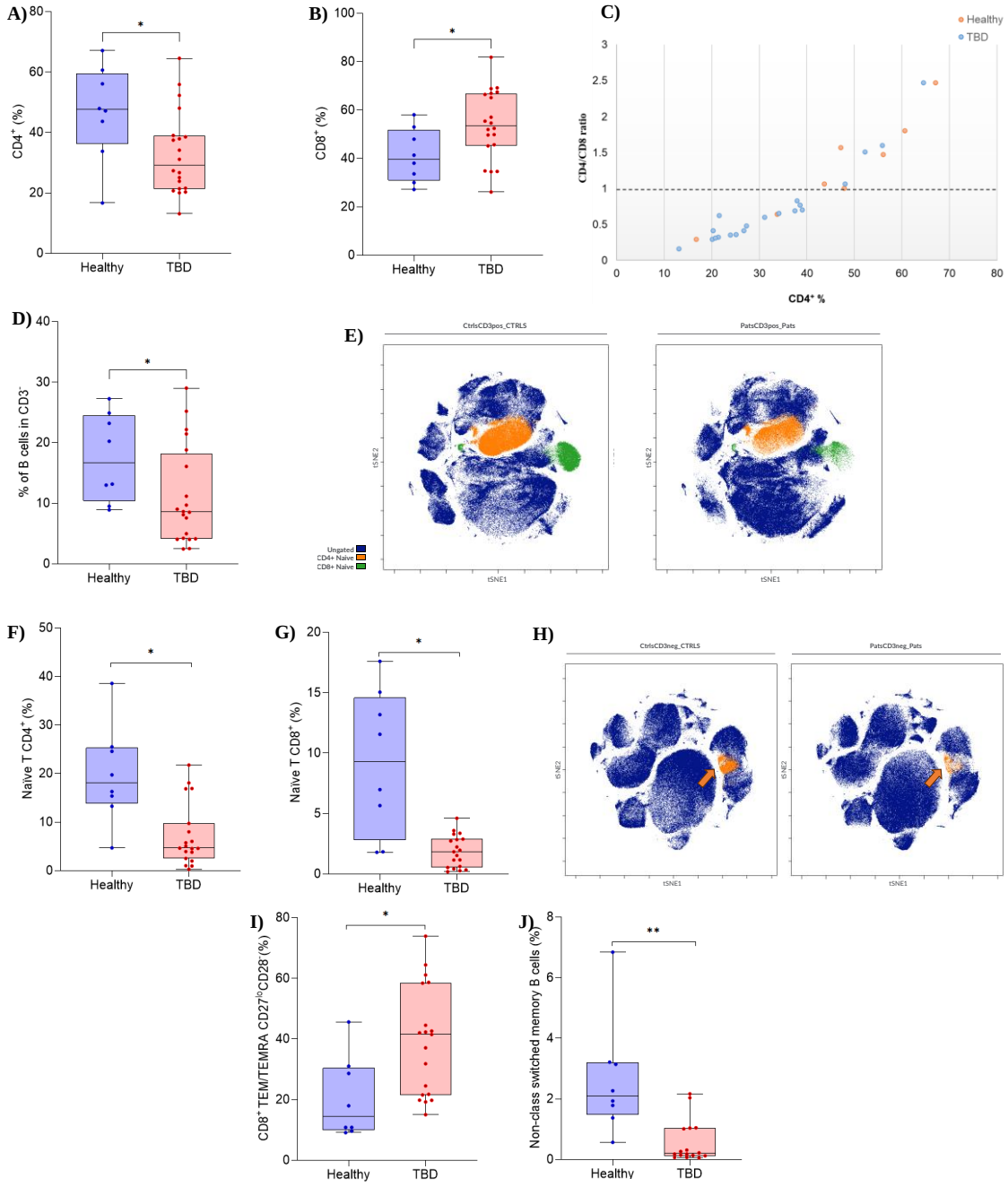

Patients with TBD present a lymphocytic phenotype compatible with premature aging. **(A** and **B)** Box plots representing the percentages of $CD4^+$ and $CD8^+$ T cells in total $CD3^+$, respectively. **(C)** CD4/CD8 ratio calculated from absolute cell counts, with the normal value being greater than 1.0. **(D)** Percentage of $CD19^+$ cells in $CD3^-$. **(E)** viSNE maps for healthy controls and TBD patients showing the naïve subsets of $CD4^+$ and $CD8^+$ cells, and $CD8^+$ TEM/TEMRA cells with $CD27^{lo}CD28^+$ phenotype. **(F** and **G)** Frequencies of naïve $CD4^+$ and $CD8^+$ cells, respectively, as defined in **(E). (H)** viSNE map highlighting a subset of non-class switched memory B cells in controls and patients. **(I** and **J)** Percentages of $CD8^+$ TEM/TEMRA $CD27^{lo}CD28^+$ cells and non-class switched memory B cells, as identified in **(E)** and **(H)**, respectively. $^*p \leq 0.05$; $^{**}p \leq 0.01$.

Figure 17. Thymic output in patients with TBD.

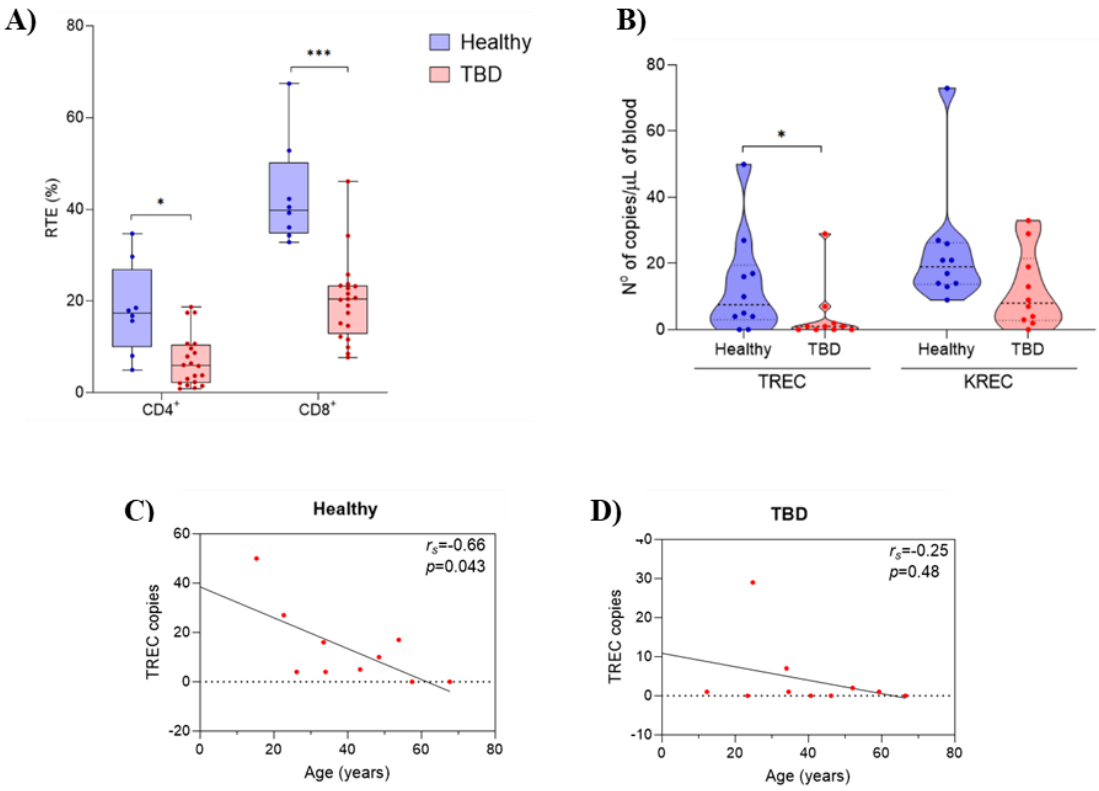

Thymus function was assessed by identifying $CD31^+CD45RA^+$ RTEs and quantifying the copy number of TRECs. KRECs were also evaluated, as indicative of B cell maturation in BM. **(A)** Percentages of $CD4^+$ and $CD8^+$ RTEs out of total $CD4^+$ and $CD8^+$, respectively. **(B)** Box plot of TRECs and KRECs copies in peripheral blood. **(C** and **D)** Spearman correlations between TREC copies and age in healthy individuals and TBD patients, respectively. $^*p \leq 0.05$; $^{***}p \leq 0.001$.

4.2.3. Poor diversity of T helper cells

As our data show, maturation of $CD4^+$ T cells is dysregulated in TBDs. Therefore, we looked into the five main subsets of T helper lymphocytes – T_H1, T_H2, T_H17, $T_H17.1$ and T_{Regs} – with the purpose of investigating whether these subpopulations were affected in telomeropathies. The T_H subsets were gated on effector cells, according to their expression of surface markers: $CD25^-CD127^+CCR6^-CXCR3^+CCR4^-$ for T_H1, $CD25^-CD127^+CCR6^-CXCR3^-CCR4^+$ for T_H2, $CD25^-CD127^+CCR6^+CXCR3^-CCR4^-$ for T_H17 and $CD25^-CD127^+CCR6^+CXCR3^+CCR4^-$ for $T_H17.1$ T_{Regs} ($CD25^+CD127^-FOXP3^+$) were identified by automated clustering. Gating

strategies for T helpers and identification of T_{Regs} by automated clustering are shown in Figures 18A-B.

T_H1, T_H17 and $T_H17.1$ subsets were found to be lower in patients, whereas T_H2/T_H1 ratio is increased when compared to controls (1.64±0.84 vs. 0.82±0.39; p=0.0063). The frequencies of T_H2 and T_{Regs} did not differ between groups (Figures 18C-D).

Figure 18. T helper subsets in TBD.

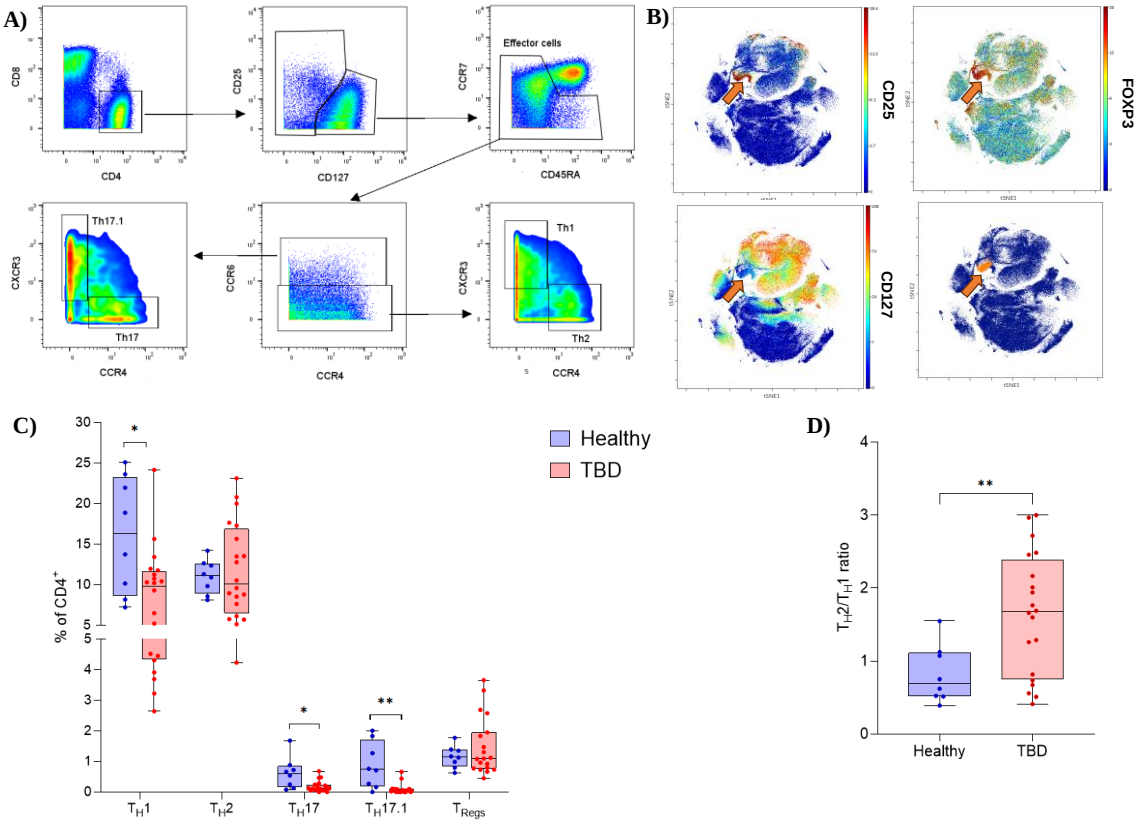

(A) Manual gating strategy for T_H1, T_H2, T_H17 and $T_H17.1$ cells. **(B)** Identification of T_{Regs} ($CD25^+CD127^-FOXP3^+$) by automated clustering. **(C)** Percentages of T helper subsets in total $CD4^+$ lymphocytes. **(D)** T_H2/T_H1 ratio is increased in patients due to the decline of T_H1 cells. $^*p\leq0.05$; $^{**}p\leq0.01$.

4.2.4. Activated and exhausted T lymphocytes, and infiltrating monocytes

A range of subpopulations expressing markers of proliferation, activation and exhaustion were identified by automated clustering. A subset of $CD4^+$ TEM cells, defined as $CD4^+CD45RA^-CCR7^-CD27^{lo}CD28^+CD38^+HLA\text{-}DR^+Ki67^+CD95^+PD\text{-}1^+CTLA\text{-}4^+$ was almost two times higher in patients than in controls (0.85 ± 0.83% of $CD3^+$ vs. 0.43 ± 0.51% of $CD3^+$; p=0.017) (Figures 19A-B). Both present in this

population, Fas (CD95) and programmed cell death 1 marker (PD-1 or CD279) are expressed following antigen-mediated T cell activation and function as regulators of apoptosis to maintain immune homeostasis (BELLESI et al., 2020). Interestingly, the frequency of $CD4^+CD95^+PD\text{-}1^+$ cells was higher in patients (13.0±6.55% of $CD4^+$ vs. 8.30±2.46% of $CD4^+$ in controls, p=0.020) and inversely correlated with $CD4^+$ T cells (r_S=-0.54; p=0.0030) and CD4/CD8 ratio (r_S=-0.53; p=0.0040). Because the same pattern was not observed for $CD8^+$ lymphocytes (Figures 19C-I)., we hypothesize that the lower frequency of $CD4^+$ T cells is due to an enhanced apoptosis caused by the overexpression of CD95 and PD-1 in TBDs.

We tested whether B cells were also overexpressing CD95 in TBDs, which was confirmed by an elevated frequency of $CD19^+CD95^+$ cells (27.0±9.83% of $CD19^+$ vs. 10.8±3.50% of $CD19^+$ in controls; p<0.0001) In a similar fashion to T cells, the relative frequency of $CD19^+CD95^+$ cells was negatively correlated with total B cells (r_S=-0.70; p<0.0001), indicating that this might be a factor that favors the decline of B lymphocytes in TBD.

Classical monocytes expressing CXCR3 ($CD14^+CD31^+CXCR3^+CCR4^+CD38^+HLA\text{-}DR^+CD39^+$) were significantly augmented in TBD patients (2.56±1.71% of $CD3^-$ vs. 0.80±0.26% of $CD3^-$ in controls; p=0.023) (Figures 19J-K). The presence of CXCR3 on the surface of monocytes is believed to be responsible for the infiltration of such cells to inflamed tissues, as its ligands CXCL9, CXCL10 and CXCL11 are upregulated in pro-inflammatory milieus (BUTLER; CLANCY-THOMPSON; MULLINS, 2017; TRAVES et al., 2016).

Figure 19. Identification of activated lymphocytes and infiltrating monocytes.

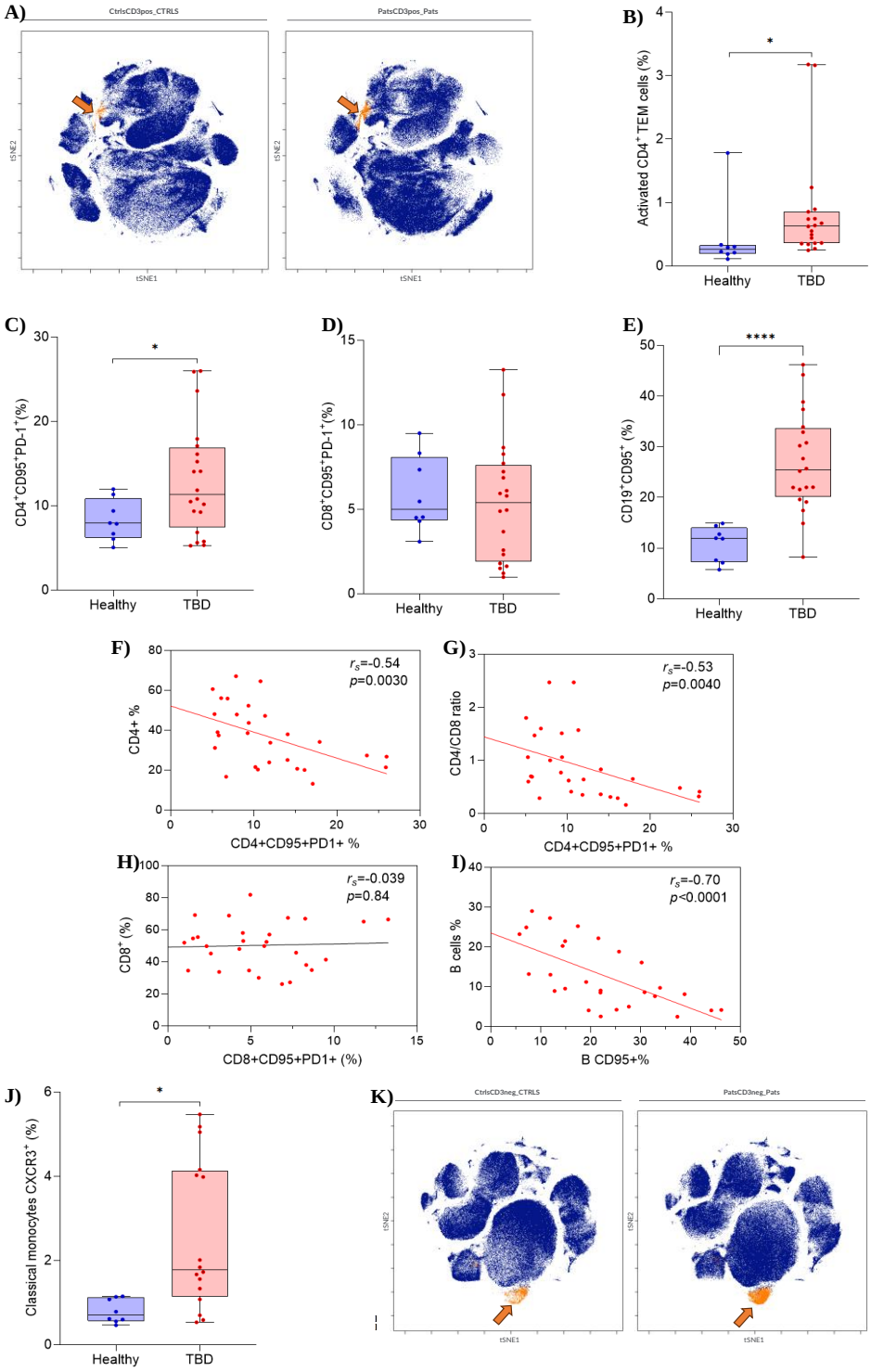

(A) viSNE map showing a population of CD4⁺ TEM activated cells being enriched in patients. **(B)** Percentages of the subset defined in **(A)**. **(C** and **D)** Expression of CD95 and PD-1 in CD4⁺ and CD8⁺ cells, respectively. **(E)** Expression of CD95 in B cells. **(F-I)** Spearman correlations between the expression of apoptosis markers and the frequencies of CD4⁺, CD8 and B cells. **(J)** Percentage of infiltrating monocytes expressing CXCR3 identified in CD3⁻ cells. **(K)** Infiltrating CXCR3⁺ monocytes highlighted on viSNE maps, with expansion in TBD patients. *$p \leq 0.05$; ****$p \leq 0.0001$.

4.2.5. Double-negative and unconventional T cells

A cluster of cytotoxic double-negative T (DNT) cells, defined as $CD3^+CD4^-CD8^-Vδ2^-CD45RA^+CCR7^-Tbet^+GZMB^+$, was found to be expanded in patients with TBD (5.67±5.75% of $CD3^+$ vs. 1.22±0.98% of $CD3^+$ in controls; p=0.017) (Figures 20A-B). This subset of $CD3^+$ cells has been closely linked with inflammatory conditions, especially autoimmune diseases (BRANDT et al., 2018; WU et al., 2022).

Another class of T cells, known as unconventional T cells due to their limited TCR diversity (GODFREY et al., 2015), was also differentially identified in patients with short telomeres. Our panel was capable of detecting two types of unconventional T cells, namely Vδ2 γδ T cells ($CD3^+CD4^-CD8^-Vδ2^+$) and MAIT cells ($CD3^+CD161^{hi}Vα7.2^+$), with both being reduced in TBD patients. First, Vδ2 γδ T cells were clustered as a very scarce population on patients' viSNE plots, as demonstrated in Figure 20B. However, the difference with the control group was not statistically significant following FDR correction (3.90±8.46% of $CD3^+$ vs. 7.42±8.2% of $CD3^+$ in controls; p=0.080). Still, it is worth noting that while healthy individuals showed a range of 0.71-27% of Vδ2 γδ T cells, 10 patients (50%), presented less than 0.5% of these cells among circulating lymphocytes (Figure 20C).

Circulating MAIT cells were markedly decreased in patients (0.12±0.15% of $CD3^+$ vs. 2.64±2.68% of $CD3^+$ in controls; p=0.0002), as shown in Figures 20B and D. As an attempt to better understand the reasons behind such decline, we collected new samples from healthy volunteers and TBD patients and performed additional flow cytometry to analyze the expression of activation and exhaustion markers in the residual cells. The frequency of MAIT cells expressing exhaustion marker CD38 was higher in patients, as well as the expression of HLA-DR (p=0.0020 for both). Concomitant expression of both markers was found in 25.5±9.74% of MAIT in patients (vs. 10.2±9.36% of MAIT in controls; p=0.0063). The frequency of $CD38^+HLA\text{-}DR^+$ MAIT cells was inversely correlated to total MAIT cells (r_S=-0.56, p=0.026), which suggests that the overactivation of this subset might be leading to its decline in peripheral blood (Figures 20E-I).

Figure 20. Frequencies of DNT and unconventional T cells.

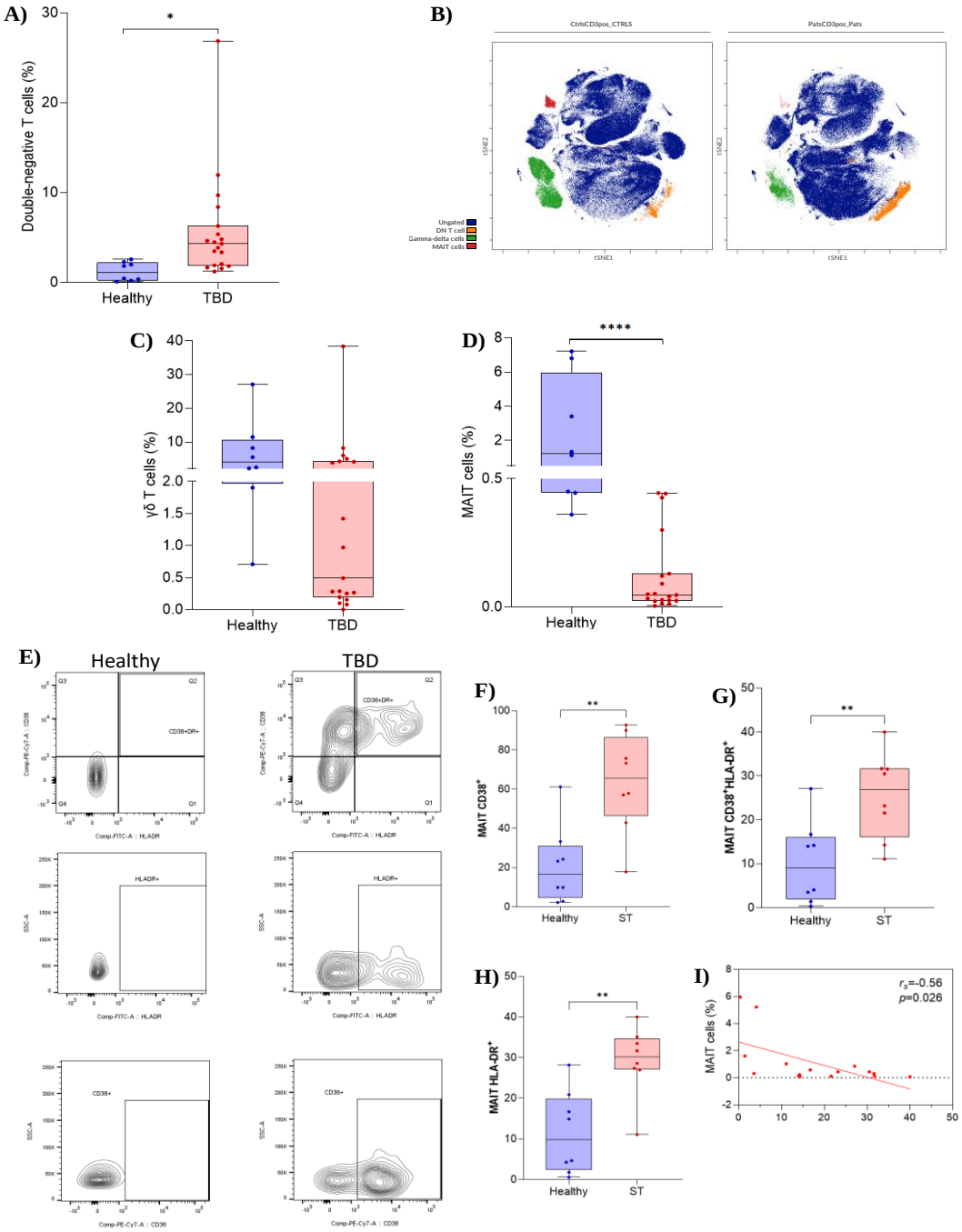

Patients with TBD exhibited alterations in minor subsets of T cells, namely DNT and unconventional T lymphocytes. **(A)** Box plot of frequencies of DNT cells, defined as $CD3^+CD4^-CD8^-V\delta2^-CD45RA^+CCR7^-Tbet^+GZMB^+$. **(B)** DNT cells, γδ and MAIT cells presented on viSNE maps of concatenated control and patient samples. **(C)** Percentage of Vδ2 γδ T cells in total $CD3^+$ lymphocytes. **(D)** MAIT cells frequencies out of total $CD3^+$ lymphocytes. **(E)** Additional flow cytometry was performed in order to assess the expression of HLA-DR and CD38 in MAIT cells, as depicted for healthy controls and TBD patients. **(F-H)** Box plots showing the percentages of expression of CD38 and HLA-DR in MAIT cells. **(I)** Spearman correlation between total circulating MAIT cells and their expression of $CD38^+HLA\text{-}DR^+$. $^*p\leq0.05$; $^{**}p\leq0.01$; $^{****}p\leq0.0001$.

4.2.6. Levels of serum cytokines, chemokines and growth factors

One of the main clinical manifestations of TBDs is pancytopenia, and our data also reveals immune alterations that are compatible with those seen in inflammatory processes. Therefore, we next aimed to assess the levels of cytokines, chemokines and growth factors in serum samples, in order to understand whether and how these proteins would be affected by the immune changes seen in TBDs.

Our Luminex™ panel was customized for 32 analytes. However, FGF-2 and IFN-α were out of range and could not be measured, resulting in 30 assessed proteins apart from TGF-β1, which was quantified by conventional ELISA. At first, none of the quantified proteins was found to have different mean concentrations in patients when compared to controls. Nonetheless, further analyses revealed that a number of cytokines, chemokines and growth factors were positively correlated to TL (z-score transformed), which shows that the shorter the telomere, the lower the levels of these biomarkers in serum (Figure 21A). Three members of the IL-1 superfamily, IL-1α, IL-1β and IL-1RA, were correlated to z-score, and total leukocytes, neutrophils, monocytes and platelets were also positively correlated to IL-1α and IL-1RA, which prompt us to infer that the decline of such cytokines is impacted by the cytopenia observed in patients. Interestingly, similar associations with such cells were found for IL-4, IL-7, MIP-3α and angiopoietin, all also correlated to TL z-score. Other analytes were also correlated to cell counts, and full associations are shown in Figure 21B.

Figure 21. Correlations of cytokines, chemokines and growth factors with z-score and blood counts.

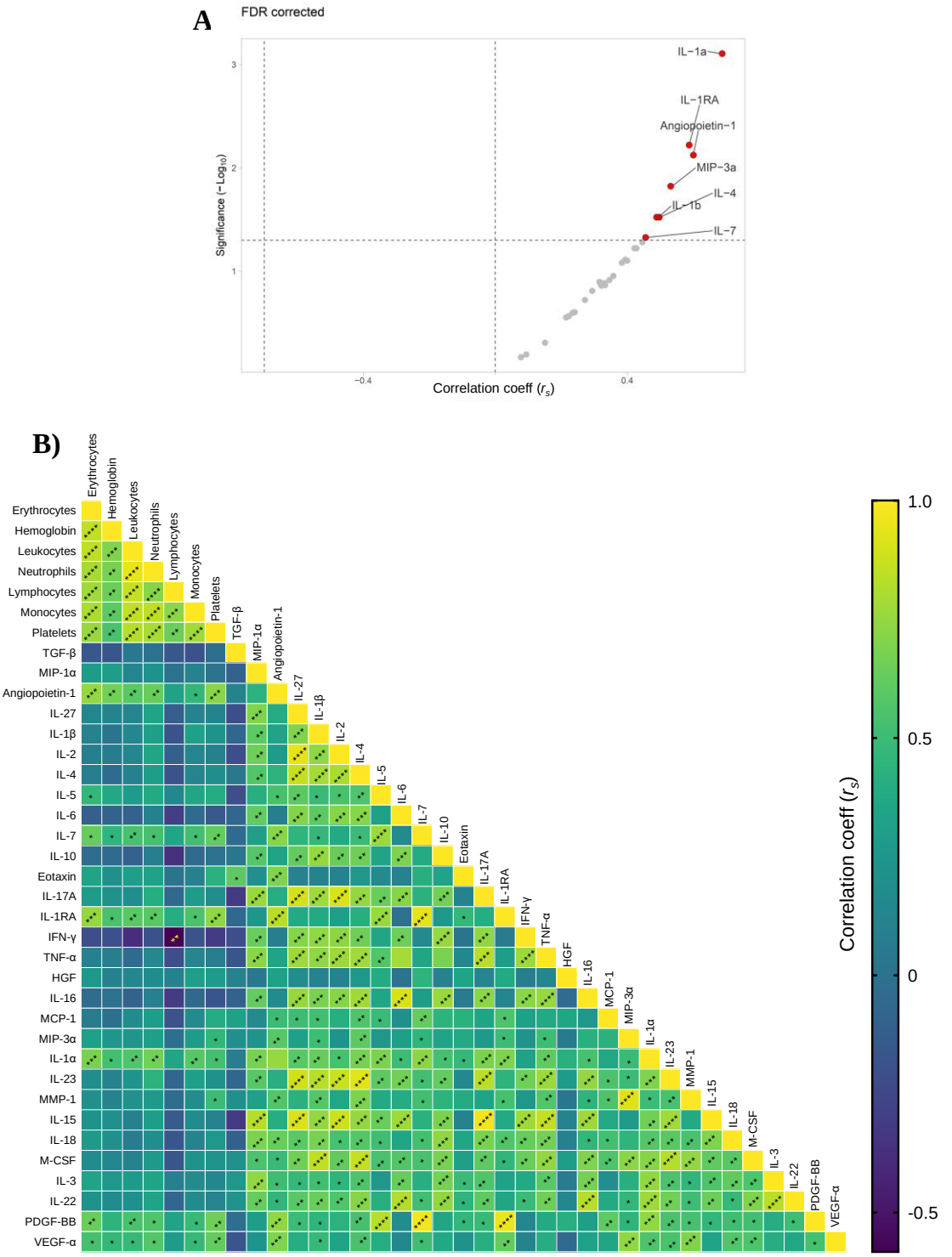

A number of analytes were correlated to TL z-score, and blood counts **(A)** Volcano plot showing data of Spearman correlations between the assessed cytokines, chemokines and growth factors versus telomere length (z-score transformed). Analytes shown in red are significantly associated with TL ($p \leq 0.050$). **(B)** Heatmap showing Spearman correlations between all analyzed analytes and blood cell counts. $^{*}p \leq 0.05$; $^{**}p \leq 0.01$; $^{***}p \leq 0.001$; $^{****}p \leq 0.0001$.

5. DISCUSSION

In this study, murine models of TBDs showed significant reduction in TL, especially in *Terc* knockouts. TL in mice is, on average, 5 to 10 times greater than that of humans (CALADO; DUMITRIU, 2013), which makes it necessary to use animals from inbreeding after successive generations, so that a significant decrease in telomeres is observed (AR et al., 2016b; PIÑEIRO-HERMIDA et al., 2020)

S. mansoni infection model was sufficient to drive liver fibrosis in our model, following 12 weeks post-inoculation of cercariae. The development of hepatic and splenic inflammation during *S. mansoni* infection is a consequence of the parasite's life cycle. Adult worms of the genus *Schistosoma* reside inside the mesenteric vessels of the intestines, feeding on nutrients present in the blood of the definitive host, such as humans or mice (COSTAIN; MACDONALD; SMITS, 2018). Once sexual maturation has been reached, male and female worms begin mating to produce approximately 300 eggs daily, per couple. These eggs must cross the endothelial barrier and the intestinal wall to reach the lumen and, finally, be excreted in the feces (COSTAIN; MACDONALD; SMITS, 2018). However, around half of the deposited eggs do not reach the intestinal lumen, but are carried by the blood flow to the liver tissue, where they cause a strong immunological reaction, leading to the formation of granulomas characterized by the infiltration of macrophages, eosinophils and T lymphocytes, in addition to proliferation of fibroblasts and production of periportal extracellular matrix (AMARAL et al., 2017; HAMS; AVIELLO; FALLON, 2013; SCHWARTZ; FALLON, 2018).

Once initiated, liver inflammation caused by *Schistosoma* eggs can progress to a chronic phase, where obstructive portal lesions, portal hypertension, hepatic encephalopathy and, finally, liver failure occur. Progressive obstruction of periportal blood flow culminates in splenomegaly due to chronic congestion and hyperplasia of the reticuloendothelial system (LLEN et al., 2002; THIJS et al., 2018).

There are no studies in the literature describing fibrosis induction in animal models of TBDs via infection with *S. mansoni* or other helminths. Therefore, additional experiments are needed to indicate the mechanisms that may be underlying the altered inflammatory response in knockout animals. Different studies suggest that telomerase, especially the TERT subunit, has an essential role in the activation of macrophages, by participating in the regulation of NF-κB (GHOSH et al., 2012; NGUYEN; WONG,

2020; WU et al., 2016). TERT directly regulates the expression of NF-κB-dependent genes by binding to the p65 subunit of NF-κB and promoting the transcription of different cytokines, such as IL-6 and TNF-α, which are critical for inflammation and, more specifically, macrophage activation. Therefore, it is plausible to infer that, in *Tert*$^{-/-}$ macrophages, this signaling pathway is impaired and cells are no longer able to respond adequately when exposed to NF-κB activating stimuli, such as *Schistosoma* infection (CHEN et al., 2020). Deficient activation of the immune system could, therefore, be a contributing factor to the lower prevalence of collagen fibers in the tissues of knockout mice, especially in the *Tert*$^{-/-}$ group, since reverse transcriptase appears to be the main subunit with non-canonical functions of the NF-κB pathway. TERC could also act as a modulator of such interaction.

In work carried out by Liu and colleagues (2007), C57BL/6 WT and *Tert*$^{-/-}$ mice, the same strains used in this study, were exposed to bleomycin to evaluate the development of pulmonary fibrosis. The results showed a lower rate of fibrosis in the lungs of knockout mice, similar to what was found in the liver tissue in the present study. The researchers reported a reduction in the expression of α-SMA in lung tissue, as well as a reduction in the proliferation capacity of fibroblasts isolated from the lungs of *Tert*$^{-/-}$ animals. The hypothesis raised was that telomerase activity is necessary for the activation of the mechanisms that support the fibrotic process, at least with regard to the chemical model used.

Deep-immunophenotyping of PBMCs from patients with short-telomere syndromes uncovered an immune signature marked by the decline of B and CD4^{+} T cells, disequilibrium of T helper lymphocytes and a higher frequency of activated and exhausted subtypes. As expected, the majority of alterations are similar to those presented in the elderly, as illustrated by the decrease of naïve subsets for both T and B cells, as well as the low TREC copies in TBD, and the accumulation of effector memory cells. Similar to what we report here, the work of Wagner et al., showed that TBD patients present an immunodeficiency marked by the decrease of naïve T cells and undetectable or low number of TRECs, having an immunophenotype comparable to individuals five decades older.

The key to the decline of naïve T cells is the thymic involution, an evolutionarily programmed process that initiates right after the first year of life and intensifies following puberty (KURIOKA; KLENERMAN, 2023; LIANG et al., 2022). Thymo-suppressive cytokines increase with age, and those include leukemia inhibitory factor,

IL-6 and oncostatin M while IL-7, a key cytokine required for thymopoiesis, decreases (LIANG et al., 2022; SEMPOWSKI et al., 2000). Interestingly, our data also show a correlation between TL and IL-7 levels in serum, suggesting that patients with very short telomeres might undergo a more intense drop of IL-7 levels.

The production of B cells is directly affected by bone marrow changes that occur with aging, which includes alterations in the HSC compartment that skew the differentiation of HSCs from lymphocytes towards myeloid cells, replacement of the hematopoietic compartment by fatty tissue and structural alterations of the stromal matrix (GEIGER; DE HAAN; CAROLINA FLORIAN, 2013; PANGRAZZI et al., 2017; TULJAPURKAR et al., 2011). Therefore, aging is associated with an overall reduction of B cells, with a shift in the proportions of B cells subsets (FRASCA et al., 2017a, 2020). The naïve ($CD19^+CD27^-IgD^+$) and unswitched memory ($CD19^+CD27^+IgD^+$) pools of B cell are usually unchanged or decreased in frequency with age, at the expense of an increased dominance of antigen-experienced and IgG^+ B cells (BULATI; CARUSO; COLONNA-ROMANO, 2017; COLONNA-ROMANO et al., 2009; FRASCA et al., 2017b; KOGUT et al., 2012), although a relative increase of naïve cells in the elderly has also been described (FRASCA et al., 2017a) In the present study, we observed a decrease of both populations in patients with telomere syndromes.

We also report aberrant proportions of T helper subsets, with the decrease of T_H1, T_H17 and $T_H17.1$ cells, but with no shifts in T_H2 and T_{Regs}. It is, thus far, not clear whether it is a bias of the differentiation stages, increased apoptosis of such cell types or a mixture of both. Intriguingly, Matthe et al. reported a preferential T_H1 in-vitro differentiation in studies with telomerase-knockout mice (MATTHE et al., 2022). Nevertheless, they did not study the differentiation towards other T_H subsets, besides having used C57BL6/J mice, known for being naturally skewed towards T_H1 phenotype (EGHOLM et al., 2022). T_H2 lymphocytes are notably enriched in cirrhotic liver and closer in proximity with collagen-producing hepatic stellate cells, being also critically important for the development of fibrosis in lungs, due to their capacity of secreting IL-4 and IL-13, both pro-fibrotic cytokines (BARRON; WYNN, 2011; DENG; HUANG; ZHANG, 2023; REISSING et al., 2024). Because TBD patients are genetically predisposed to liver cirrhosis and IPF, the relationship between the imbalanced T_H2/T_H1 ratio we reported here and the development of such complications should be addressed in future studies.

A rare subset of $CD4^+$ lymphocytes, defined as $CD4^+CD45RA^-CCR7^-CD27^{lo}CD28^+CD38^+HLA\text{-}DR^+Ki67^+CD95^+PD\text{-}1^+CTLA\text{-}4^+$ was elevated in TBD patients. The presence of HLA-DR, Ki67, PD-1 and CD38 indicate that this population is activated and undergoing proliferation. The expression of HLA-DR by CD4+ T cells has been attributed to inflammatory processes, including autoimmune and infectious diseases (AHMED et al., 2018; MEDITZ et al., 2011; VIALLARD et al., 2001). This subtype still expresses CD27 and CD28, showing that it is not impacted by immunosenescence yet, as the progressive loss of these receptors is directly correlated with immunological aging (LARBI; FULOP, 2014); the presence of proliferation marker Ki67 corroborates with this point. This suggests that, despite the overall indication of an aged immune system, remaining functional effector memory T cells could be chronically activated in TBD patients.

The low frequency of circulating MAIT cells, as seen in patients with TBD, is also a potential indicator of ongoing inflammatory processes in the body. Aging also seems to play a role in MAIT cells decreasing, but only to a certain extent. Chen et al., (2019) reported an increase in MAIT cells activation in peripheral blood, and lower percentages of these cells in individuals over 60 years of age. The mean frequency ± SEM of MAIT cells in this population was 0.56±0.07% of $CD3^+$ against 1.51±0.13% of $CD3^+$ in subjects with ages from 20 to 40 years. Similar results were found by other groups that studied the dynamics of MAIT cells though aging (LOH et al., 2020; NOVAK et al., 2014). Our study, however, showed that TBD patients have even lower percentages, with an average of 0.12% of MAIT cells in $CD3^+$ population, with 58% of patients presenting a frequency of less than 0.05%. Recently, it has been shown that MAIT cells in the elderly had higher expression of markers such as granzyme-B and IFN-γ at baseline, and suggested that there is a low-grade basal inflammatory activation of these cells in old age (LOH et al., 2020). It is possible that the so called “inflamm-aging” is also taking place in telomere diseases, but other hypotheses should be tested in order to clarify this phenomenon. The migration of these cells from peripheral blood to inflamed tissues has also been proposed, in an attempt to explain the drops observed in circulating MAIT cells in inflammatory diseases. However, no consensus has been reached yet. The accumulation of MAIT cells in tissues has been observed for some disorders, as in bacterial pulmonary infection, ulcerative colitis and multiple sclerosis (CHEN et al., 2017; HAGA et al., 2016; ILLÉS et al., 2004; MEIEROVICS; YANKELEVICH; COWLEY, 2013). Interestingly, despite being

naturally enriched in the liver, corresponding up to 45% of T lymphocytes in healthy conditions (DUSSEAUX et al., 2011; TANG et al., 2013), expansion of MAIT cells in the inflamed liver has rarely been found, with their levels frequently being decreased (BOLTE et al., 2017; BÖTTCHER et al., 2018; MABIRE et al., 2023; NIEHAUS et al., 2020). However, their role in hepatic fibrosis is regarded as important, as they accumulate in fibrotic septa and interact with pro-fibrotic macrophages (HEGDE et al., 2018; MABIRE et al., 2023).

6. CONCLUSION

Short telomere syndromes are known for causing a range of clinical manifestations in several organs, as a consequence of premature senescence and exhaustion of stem cells. Lung and liver fibrosis remain as frequent complications in patients with TBDs, although the mechanisms underlying such manifestations are unclear. In this study, we show immune dysregulation in patients with short telomeres, marked by CD4 T cell immunodeficiency, as well as a reduction in B cells, naïve lymphocytes and unconventional T cells. Activated and exhausted lymphocytes were also frequent, which implies that an inflammatory milieu might be chronically stimulated by cellular senescence.

Our murine model corroborates with the hypothesis of a dysregulated immune system. Interestingly, the model chosen for liver fibrosis development seems to be dependent of telomerase, as macrophages, key cells in the pro-fibrotic response, are no longer activated in the absence of TERT or TERC. Our data opens several new questions that must be addressed in future studies so we can understand the mechanisms behind the alterations observed.

7. REFERENCES

AHMED, A.; ADIGA, V.; NAYAK, S.; UDAY KUMAR, J. A. J.; DHAR, C.; SAHOO, P. N.; SUNDARARAJ, B. K.; SOUZA, G. D.; VYAKARNAM, A. Circulating HLA-DR+CD4+ effector memory T cells resistant to CCR5 and PD-L1 mediated suppression compromise regulatory T cell function in tuberculosis. PLoS Pathogens, v. 14, n. 9, 1 set. 2018.

ALVES-PAIVA, R. M.; KAJIGAYA, S.; FENG, X.; CHEN, J.; DESIERTO, M.; WONG, S.; TOWNSLEY, D. M.; DONAIRES, F. S.; BERTOLA, A.; GAO, B.; YOUNG, N. S.; CALADO, R. T. Telomerase enzyme deficiency promotes metabolic dysfunction in murine hepatocytes upon dietary stress. Liver International, v. 38, n. 1, p. 144–154, 1 jan. 2018.

AMARAL, K. B.; SILVA, T. P.; DIAS, F. F.; MALTA, K. K.; ROSA, F. M.; COSTA-NETO, S. F.; GENTILE, R.; MELO, R. C. N. Histological assessment of granulomas in natural and experimental Schistosoma mansoni infections using whole slide imagingPLoS ONEPublic Library of Science, 1 set. 2017.

AMIR, E. A. D.; DAVIS, K. L.; TADMOR, M. D.; SIMONDS, E. F.; LEVINE, J. H.; BENDALL, S. C.; SHENFELD, D. K.; KRISHNASWAMY, S.; NOLAN, G. P.; PE'ER, D. ViSNE enables visualization of high dimensional single-cell data and reveals phenotypic heterogeneity of leukemia. Nature Biotechnology, v. 31, n. 6, p. 545–552, jun. 2013.

AR, C. B. ¨; POVEDANO, J. M.; SERRANO, R.; BENITEZ-BUELGA, C.; POPKES, M.; FORMENTINI, I.; BOBADILLA, M.; BOSCH, F.; BLASCO, M. A. Telomerase gene therapy rescues telomere length, bone marrow aplasia, and survival in mice with aplastic anemia. 2016a.

ARISH, N.; PETUKHOV, D.; WALLACH-DAYAN, S. B. The role of telomerase and telomeres in interstitial lung diseases: From molecules to clinical implications. International Journal of Molecular Sciences, v. 20, n. 12, 2 jun. 2019.

AUBERT, G.; LANSDORP, P. M. Telomeres and agingPhysiological Reviewsabr. 2008.

BALL, S.E.; GIBSON, F.M.; RIZZO, S.; TOOZE, J.A.; MARSH, J.C.; GORDON-SMITH, E.C. Progressive telomere shortening in aplastic anemia. Blood. v. 91, n. 10, p. 3582-3592; 1998.

BARRON, L.; WYNN, T. A. Fibrosis is regulated by Th2 and Th17 responses and by dynamic interactions between fibroblasts and macrophages. Am J Physiol Gastro-intest Liver Physiol, v. 300, p. 723–728, 2011.

BERTUCH, A. A. The molecular genetics of the telomere biology disordersRNA BiologyTaylor and Francis Inc., 2 ago. 2016.

BILGILI, H.; BIAŁAS, A. J.; GÓRSKI, P.; PIOTROWSKI, W. J. Telomere abnormalities in the pathobiology of idiopathic pulmonary fibrosisJournal of Clinical MedicineMDPI, 1 ago. 2019a.

BILGILI, H.; BIAŁAS, A. J.; GÓRSKI, P.; PIOTROWSKI, W. J. Telomere abnormalities in the pathobiology of idiopathic pulmonary fibrosisJournal of Clinical MedicineMDPI, 1 ago. 2019b.

BOLTE, F. J.; O'KEEFE, A. C.; WEBB, L. M.; SERTI, E.; RIVERA, E.; LIANG, T. J.; GHANY, M.; REHERMANN, B. Intra-Hepatic Depletion of Mucosal-Associated Invariant T Cells in Hepatitis C Virus-Induced Liver Inflammation. Gastroenterology, v. 153, n. 5, p. 1392- 1403.e2, 1 nov. 2017.

BORTE, S.; VON DÖBELN, U.; FASTH, A.; WANG, N.; JANZI, M.; WINIARSKI, J.; SACK, U.; PAN-HAMMARSTRÖM, Q.; BORTE, M.; HAMMARSTRÖM, L. Neonatal screening for severe primary immunodeficiency diseases using high-throughput triplex real-time PCR. Blood, v. 119, n. 11, p. 2552–2555, 15 mar. 2012.

BÖTTCHER, K.; ROMBOUTS, K.; SAFFIOTI, F.; ROCCARINA, D.; ROSSELLI, M.; HALL, A.; LUONG, T. V.; TSOCHATZIS, E. A.; THORBURN, D.; PINZANI, M. MAIT cells are chronically activated in patients with autoimmune liver disease and promote profibrogenic hepatic stellate cell activation. Hepatology, v. 68, n. 1, p. 172–186, 1 jul. 2018.

BULATI, M.; CARUSO, C.; COLONNA-ROMANO, G. From lymphopoiesis to plasma cells differentiation, the age-related modifications of B cell compartment are influenced by "inflamm-ageing"Ageing Research Reviews. Elsevier Ireland Ltd, 1 jul. 2017.

BUTLER, K. L.; CLANCY-THOMPSON, E.; MULLINS, D. W. CXCR3 + monocytes/macrophages are required for establishment of pulmonary metastases. Scientific Reports, v. 7, 30 mar. 2017.

CALADO, R. T.; BRUDNO, J.; MEHTA, P.; KOVACS, J. J.; WU, C.; ZAGO, M. A.; CHANOCK, S. J.; BOYER, T. D.; YOUNG, N. S. Constitutional telomerase mutations are genetic risk factors for cirrhosis. Hepatology, v. 53, n. 5, p. 1600–1607, 2011.

CALADO, R. T.; DUMITRIU, B. Telomere dynamics in mice and humans. Seminars in Hematology, v. 50, n. 2, p. 165–174, abr. 2013.

CALADO, R. T.; YOUNG, N. S. Telomere Diseases. N Engl J Med. v. 361, n. 24, p. 2353- 2365; 2009.

CAO, S.; YAQOOB, U.; DAS, A.; SHERGILL, U.; JAGAVELU, K.; HUEBERT, R. C.; ROUTRAY, C.; ABDELMONEIM, S.; VASDEV, M.; LEOF, E.; CHARLTON, M.; WATTS, R. J.; MUKHOPADHYAY, D.; SHAH, V. H. Neuropilin-1 promotes cirrhosis of the rodent and human liver by enhancing PDGF/TGF-β signaling in hepatic stellate cells. Journal of Clinical Investigation, v. 120, n. 7, p. 2379–2394, 1 jul. 2010.

CARULLI, L. Telomere shortening as genetic risk factor of liver cirrhosisWorld Journal of GastroenterologyWJG Press, 14 jan. 2015.

CARVALHO, V. S.; GOMES, W. R.; CALADO, R. T. Recent advances in understanding telomere diseases. Faculty Reviews, v. 11, 19 out. 2022.

CHEEVER, A. W.; LENZI, J. A.; LENZI, H. L.; ANDRADE, Z. A. Experimental models of

Schistosoma mansoni infection. Mem. Inst. Oswaldo Cruz. v. 97, n. 7, p. 917-940; 2002.

CHEN, P.; DENG, W.; LI, D.; ZENG, T.; HUANG, L.; WANG, Q.; WANG, J.; ZHANG, W.; YU, X.; DUAN, D.; WANG, J.; XIA, H.; CHEN, H.; HUANG, W.; LI, J.; ZHANG, D.; ZHONG, X. P.; GAO, J. Circulating mucosal-associated invariant T Cells in a large cohort of chiniese individuals from newborn to elderly. Frontiers in Immunology, v. 10, n. FEB, 2019.

CHEN, R.; ZHANG, K.; CHEN, H.; ZHAO, X.; WANG, J.; LI, L.; CONG, Y.; JU, Z.; XU, D.; WILLIAMS, B. R. G.; JIA, J.; LIU, J. P. Telomerase deficiency causes alveolar stem cell senescence-associated low-grade inflammation in lungs. Journal of Biological Chemistry, v. 290, n. 52, p. 30813–30829, 25 dez. 2015.

CHEN, T. T. W.; CHENG, P. C.; CHANG, K. C.; CAO, J. P.; FENG, J. L.; CHEN, C. C.; LAM, H. Y. P.; PENG, S. Y. Activation of the NLRP3 and AIM2 inflammasomes in a mouse model of Schistosoma mansoni infection. Journal of Helminthology, v. 94, 2020.

CHEN, Z.; WANG, H.; D'SOUZA, C.; SUN, S.; KOSTENKO, L.; ECKLE, S. B. G.; MEEHAN, B. S.; JACKSON, D. C.; STRUGNELL, R. A.; CAO, H.; WANG, N.; FAIRLIE, D. P.; LIU, L.; GODFREY, D. I.; ROSSJOHN, J.; MCCLUSKEY, J.; CORBETT, A. J. Mucosal-associated invariant T-cell activation and accumulation after in vivo infection depends on microbial riboflavin synthesis and co-stimulatory signals. Mucosal Immunology, v. 10, n. 1, p. 58–68, 1 jan. 2017.

COLONNA-ROMANO, G.; BULATI, M.; AQUINO, A.; PELLICANÒ, M.; VITELLO, S.; LIO, D.; CANDORE, G.; CARUSO, C. A double-negative (IgD-CD27-) B cell population is increased in the peripheral blood of elderly people. Mechanisms of Ageing and Development, v. 130, n. 10, p. 681–690, out. 2009.

COSTAIN, A. H.; MACDONALD, A. S.; SMITS, H. H. Schistosome Egg Migration: Mechanisms, Pathogenesis and Host Immune Responses Frontiers in Immunology. Frontiers Media S.A., 20 dez. 2018.

CRESPO YANGUAS, S.; COGLIATI, B.; WILLEBRORDS, J.; MAES, M.; COLLE, I.; VAN DEN BOSSCHE, B.; DE OLIVEIRA, C. P. M. S.; ANDRAUS, W.; ALVES, V. A.; LECLERCQ, I.; VINKEN, M. Experimental models of liver fibrosis Archives of Toxicology. Springer Verlag, 2016.

CUI, Q.; WANG, Z.; JIANG, D.; QU, L.; GUO, J.; LI, Z. HGF inhibits TGF-β1-induced myofibroblast differentiation and ECM deposition via MMP-2 in Achilles tendon in rat. European Journal of Applied Physiology, v. 111, n. 7, p. 1457–1463, jul. 2011.

DENG, L.; HUANG, T.; ZHANG, L. T cells in idiopathic pulmonary fibrosis: crucial but controversialCell Death Discovery. Springer Nature, 2023.

DONAIRES, F. S.; SCATENA, N. F.; ALVES-PAIVA, R. M.; PODLEVSKY, J. D.; LOGESWARAN, D.; SANTANA, B. A.; TEIXEIRA, A. C.; CHEN, J. J. L.; CALADO, R. T.; MARTINELLI, A. L. C. Telomere biology and telomerase mutations in cirrhotic patients with hepatocellular carcinoma. PLoS ONE, v. 12, n. 8, 1 ago. 2017.

DU, W. J.; ZHEN, J. H.; ZENG, Z. Q.; ZHENG, Z. M.; XU, Y.; QIN, L. Y.; CHEN, S. J. Expression of Interleukin-17 associated with disease progression and liver fibrosis with hepatitis B virus infection: IL-17 in HBV infection. Diagnostic Pathology, v. 8, n. 1, 28 fev. 2013.

DUSSEAUX, M.; MARTIN, E.; SERRIARI, N.; PÉ GUILLET, I.; PREMEL, V.; LOUIS, D.; MILDER, M.; LE BOURHIS, L.; SOUDAIS, C.; TREINER, E.; LANTZ, O. Human MAIT cells are xenobiotic-resistant, tissue-targeted, CD161 hi IL-17-secreting T cells. v. 117, n. 4, p. 1250–1259, 2011.

EGHOLM, C.; ÖZCAN, A.; BREU, D.; BOYMAN, O. Type 2 immune predisposition results in accelerated neutrophil aging causing susceptibility to bacterial infection Sci. Immunol. 2022.

FERNÁNDEZ GARCÍA, M. S.; TERUYA-FELDSTEIN, J. The diagnosis and treatment of dyskeratosis congenita: A reviewJournal of Blood Medicine. Dove Medical Press Ltd, 2014.

FORTEA, J. I.; FERNÁNDEZ-MENA, C.; PUERTO, M.; RIPOLL, C.; ALMAGRO, J.; BAÑARES, J.; BELLÓN, J. M.; BAÑARES, R.; VAQUERO, J. Comparison of Two Protocols of Carbon Tetrachloride-Induced Cirrhosis in Rats - Improving Yield and Reproducibility. Scientific Reports, v. 8, n. 1, 1 dez. 2018.

FRASCA, D.; DIAZ, A.; ROMERO, M.; BLOMBERG, B. B. Human peripheral late/exhausted memory B cells express a senescent-associated secretory phenotype and preferentially utilize metabolic signaling pathways. Experimental Gerontology, v. 87, p. 113–120, 1 jan. 2017a.

FRASCA, D.; DIAZ, A.; ROMERO, M.; D'ERAMO, F.; BLOMBERG, B. B. Aging effects on T-bet expression in human B cell subsets. Cellular Immunology, v. 321, p. 68–73, 1 nov. 2017b.

FRASCA, D.; DIAZ, A.; ROMERO, M.; GARCIA, D.; BLOMBERG, B. B. Annual Review of Cell and Developmental Biology B Cell Immunosenescence. 2020.

FRIEDMAN, S. L. Molecular Regulation of Hepatic Fibrosis, an Integrated Cellular Response to Tissue Injury*. J Biol Chem. 28;275(4):2247-50; 2000.

GANDHI, C. R. Chapter 14 - Stellate Cells in Hepatic Immunological Tolerance. *Em*: Stellate Cells in Health and Disease. [s.l.] Elsevier Inc., 2015. p. 227–250.

GANDHI, C. R. Hepatic stellate cell activation and pro-fibrogenic signalsJournal of HepatologyElsevier B.V., 1 nov. 2017.

GEIGER, H.; DE HAAN, G.; CAROLINA FLORIAN, M. The ageing haematopoietic stem cell compartmentNature Reviews Immunology; 2013.

GHOSH, A.; SAGINC, G.; LEOW, S. C.; KHATTAR, E.; SHIN, E. M.; YAN, T. D.; WONG, M.; ZHANG, Z.; LI, G.; SUNG, W. K.; ZHOU, J.; CHNG, W. J.; LI, S.; LIU, E.; TERGAONKAR, V. Telomerase directly regulates NF-B-dependent transcription. Nature Cell Biology, v. 14, n. 12, p. 1270–1281, dez. 2012.

GIELING, R. G.; WALLACE, K.; HAN, Y. P. Interleukin-1 participates in the progression from liver injury to fibrosis. American Journal of Physiology - Gastrointestinal and Liver Physiology, v. 296, n. 6, jun. 2009.

GIESECK, R. L.; WILSON, M. S.; WYNN, T. A. Type 2 immunity in tissue repair and fibrosisNature Reviews Immunology Nature Publishing Group, 2018.

GIULIO ROMANELLI, R.; STASI, C. Recent Advancements in Diagnosis and Therapy of Liver Cirrhosis. Current Drug Targets, v. 17, n. 15, p. 1804–1817, 25 jun. 2016.

GODFREY, D. I.; ULDRICH, A. P.; MCCLUSKEY, J.; ROSSJOHN, J.; MOODY, D. B. The burgeoning family of unconventional T cellsNature ImmunologyNature Publishing Group, 20 out. 2015.

GRAMATGES, M. M.; BERTUCH, A. A. Short telomeres: From dyskeratosis congenita to sporadic aplastic anemia and malignancyTranslational Research. Mosby Inc., 2013.

GUTIERREZ-RODRIGUES, F.; SANTANA-LEMOS, B. A.; SCHEUCHER, P. S.; ALVES-PAIVA, R. M.; CALADO, R. T. Direct comparison of Flow-FISH and qPCR as diagnostic tests for telomere length measurement in humans. PLoS ONE, v. 9, n. 11, 19 nov. 2014.

HAGA, K.; CHIBA, A.; SHIBUYA, T.; OSADA, T.; ISHIKAWA, D.; KODANI, T.; NOMURA, O.; WATANABE, S.; MIYAKE, S. MAIT cells are activated and accumulated in the inflamed mucosa of ulcerative colitis. Journal of Gastroenterology and Hepatology (Australia), v. 31, n. 5, p. 965–972, 2016.

HAMS, E.; AVIELLO, G.; FALLON, P. G. The Schistosoma granuloma: Friend or foe? Frontiers in Immunology, v. 4, n. APR, 2013.

HARTMANN, D.; SRIVASTAVA, U.; THALER, M.; KLEINHANS, K. N.; N'KONTCHOU, G.; SCHEFFOLD, A.; BAUER, K.; KRATZER, R. F.; KLOOS, N.; KATZ, S. F.; SONG, Z.; BEGUS-NAHRMANN, Y.; KLEGER, A.; VON FIGURA, G.; STRNAD, P.; LECHEL, A.; GÜNES, C.; POTTHOFF, A.; DETERDING, K.; WEDEMEYER, H.; JU, Z.; SONG, G.; XIAO, F.; GILLEN, S.; SCHREZENMEIER, H.; MERTENS, T.; ZIOL, M.; FRIESS, H.; JAREK, M.; MANNS, M. P.; BEAUGRAND, M.; RUDOLPH, K. L. Telomerase gene mutations are associated with cirrhosis formation. Hepatology, v. 53, n. 5, p. 1608–1617, 2011.

HEGDE, P.; WEISS, E.; PARADIS, V.; WAN, J.; MABIRE, M.; SUKRITI, S.; RAUTOU, P. E.; ALBUQUERQUE, M.; PICQ, O.; GUPTA, A. C.; FERRERE, G.; GILGENKRANTZ, H.; KIAF, B.; TOUBAL, A.; BEAUDOIN, L.; LETTÉRON, P.; MOREAU, R.; LEHUEN, A.; LOTERSZTAJN, S. Mucosal-associated invariant T cells are a profibrogenic immune cell population in the liver. Nature Communications, v. 9, n. 1, 1 dez. 2018.

Heiss et al. X-linked dyskeratosis congenita is caused by mutations in a highly conserved gene with putative nucleolar functions. 19(1):32-8; 1998.

HOLOHAN, B.; WRIGHT, W. E.; SHAY, J. W. Telomeropathies: An emerging spectrum disorderJournal of Cell Biology. Rockefeller University Press, 2014.

ILLÉS, Z.; SHIMAMURA, M.; NEWCOMBE, J.; OKA, N.; YAMAMURA, T. Accumulation of Vα7.2-Jα33 invariant T cells in human autoimmune inflammatory

lesions in the nervous system. International Immunology, v. 16, n. 2, p. 223–230, fev. 2004.

IWAKIRI, Y. Pathophysiology of portal hypertensionClinics in Liver DiseaseW.B. Saunders, 2014.

JUNQUEIRA, L. C. U.; BIGNOLAS, G.; BRENTANI, R. R. Picrosirius staining plus polarization microscopy, a specific method for collagen detection in tissue sections. Histochemicat Journal. 1978.

KAMARI, Y.; SHAISH, A.; VAX, E.; SHEMESH, S.; KANDEL-KFIR, M.; ARBEL, Y.; OLTEANU, S.; BARSHACK, I.; DOTAN, S.; VORONOV, E.; DINARELLO, C. A.; APTE, R. N.; HARATS, D. Lack of interleukin-1α or interleukin-1β inhibits transformation of steatosis to steatohepatitis and liver fibrosis in hypercholesterolemic mice. Journal of Hepatology, v. 55, n. 5, p. 1086–1094, nov. 2011.

KAMINSKI, N.; ALLARD, J. D.; PITTET, J. F.; ZUO, F.; GRIFFITHS, M. J. D.; MORRIS, D.; HUANG, X.; SHEPPARD, D.; HELLER, R. A. Global analysis of gene expression in pulmonary fibrosis reveals distinct programs regulating lung inflammation and fibrosis. 15;97(4):1778-83; 2000.

KANEGAE, M. P. P.; BARREIROS, L. A.; SOUSA, J. L.; BRITO, M. A. S.; DE OLIVEIRA, E. B.; SOARES, L. P.; MAZZUCCHELLI, J. T. L.; FERNANDES, D. Q.; HADACHI, S. M.; HOLANDA, S. M.; GUIMARÃES, F. A. T. M.; BOACNIN, M. A. P. V. V.; PEREIRA, M. A. L.; BUENO, J. M. C.; GRUMACH, A. S.; DI GESU, R. S. W.; DOS SANTOS, A. M. N.; BELLESI, N.; COSTA-CARVALHO, B. T.; CONDINO-NETO, A. Newborn screening for severe combined immunodeficiencies using trecs and krecs: Second pilot study in Brazil. Revista Paulista de Pediatria, v. 35, n. 1, p. 25–32, 1 jan. 2017.

KHAWAR, M. B.; AZAM, F.; SHEIKH, N.; ABDUL MUJEEB, K. How Does Interleukin-22 Mediate Liver Regeneration and Prevent Injury and Fibrosis?Journal of Immunology ResearchHindawi Publishing Corporation, 2016.

KIRWAN, M.; DOKAL, I. Dyskeratosis congenita, stem cells and telomeresBiochimica et Biophysica Acta - Molecular Basis of Diseaseabr. 2009.

KOGUT, I.; SCHOLZ, J. L.; CANCRO, M. P.; CAMBIER, J. C. B cell maintenance and function in agingSeminars in Immunologyout. 2012.

KOMOHARA, Y.; NAKAGAWA, T.; OHNISHI, K.; KOSAKI, Y.; SAITO, Y.; HORLAD, H.; FUJIWARA, Y.; TAKEYA, M. Optimum immunohistochemical procedures for analysis of macrophages in human and mouse formalin fixed paraffin-embedded tissue samplesJournal of clinical and experimental hematopathology. 2017.

KURIOKA, A.; KLENERMAN, P. Aging unconventionally: γδ T cells, iNKT cells, and MAIT cells in agingSeminars in Immunology. Academic Press, 1 set. 2023.

Laish et al. Telomere Length, Aggregates, and Capture in Cirrhosis. Isr Med Assoc J . 20(5):295-299; 2018.

LARBI, A.; FULOP, T. From “truly naïve” to “exhausted senescent” T cells: When markers predict functionalityCytometry Part A; 2014.

LIANG, Z.; DONG, X.; ZHANG, Z.; ZHANG, Q.; ZHAO, Y. Age-related thymic involution: Mechanisms and functional impactAging Cell. John Wiley and Sons Inc, 1 ago. 2022.

LIU, T.; MYOUNG, J. C.; ULLENBRUCH, M.; YU, H.; JIN, H.; HU, B.; YOON, Y. C.; ISHIKAWA, F.; PHAN, S. H. Telomerase activity is required for bleomycin-induced pulmonary fibrosis in mice. Journal of Clinical Investigation, v. 117, n. 12, p. 3800–3809, dez. 2007.

LIU, X.; HU, H.; YIN, J. Q. Therapeutic strategies against TGF-β signaling pathway in hepatic fibrosisLiver International. 2006.

LIU, Y. ying; SHI, Y.; LIU, Y.; PAN, X. hua; ZHANG, K. xiong. Telomere shortening activates TGF-β/Smads signaling in lungs and enhances both lipopolysaccharide and bleomycin-induced pulmonary fibrosis. Acta Pharmacologica Sinica, v. 39, n. 11, p. 1735–1745, 1 nov. 2018.

LLEN, A.; OSS, G. P. R.; ARTLEY, A. B. B.; DRIAN, A.; LEIGH, C. S.; ICHARD, G. R.; LDS, O.; UESHENG L I, Y.; AIL, G.; ILLIAMS, M. W.; ANUS, M. SCHISTOSOMIASIS. N E J Med. 2022.

LOH, L.; GHERARDIN, N. A.; SANT, S.; GRZELAK, L.; CRAWFORD, J. C.; BIRD, N. L.; KOAY, H.-F.; VAN DE SANDT, C. E.; MOREIRA, M. L.; LAPPAS, M.; ALLEN, E. K.; CROWE, J.; LOUDOVARIS, T.; FLANAGAN, K. L.; QUINN, K. M.; ROSSJOHN, J.; THOMAS, P. G.; ECKLE, S. B. G.; MCCLUSKEY, J.; GODFREY, D. I.; KEDZIERSKA, K. Human Mucosal-Associated Invariant T Cells in Older Individuals Display Expanded TCRαβ Clonotypes with Potent Antimicrobial Responses. The Journal of Immunology, v. 204, n. 5, p. 1119–1133, 1 mar. 2020.

LU, W.; ZHANG, Y.; LIU, D.; SONGYANG, Z.; WAN, M. Telomeres-structure, function, and regulationExperimental Cell ResearchAcademic Press Inc., 15 jan. 2013.

MABIRE, M.; HEGDE, P.; HAMMOUTENE, A.; WAN, J.; CAËR, C.; SAYEGH, R. Al; CADOUX, M.; ALLAIRE, M.; WEISS, E.; THIBAULT-SOGORB, T.; LANTZ, O.; GOODHARDT, M.; PARADIS, V.; DE LA GRANGE, P.; GILGENKRANTZ, H.; LOTERSZTAJN, S. MAIT cell inhibition promotes liver fibrosis regression via macrophage phenotype reprogramming. Nature Communications, v. 14, n. 1, 1 dez. 2023.

MARTIN, I. V.; BORKHAM-KAMPHORST, E.; ZOK, S.; VAN ROEYEN, C. R. C.; ERIKSSON, U.; BOOR, P.; HITTATIYA, K.; FISCHER, H. P.; WASMUTH, H. E.; WEISKIRCHEN, R.; EITNER, F.; FLOEGE, J.; OSTENDORF, T. Platelet-derived growth factor (PDGF)-C neutralization reveals differential roles of PDGF receptors in liver and kidney fibrosis. American Journal of Pathology, v. 182, n. 1, p. 107–117, jan. 2013.

MARTINEZ, F. J.; CHISHOLM, A.; COLLARD, H. R.; FLAHERTY, K. R.; MYERS, J.; RAGHU, G.; WALSH, S. L. F.; WHITE, E. S.; RICHELDI, L. The diagnosis of idiopathic pulmonary fibrosis: current and future approachesThe Lancet Respiratory MedicineLancet Publishing Group, 1 jan. 2017.

MATTHE, D. M.; THOMA, O. M.; SPERKA, T.; NEURATH, M. F.; WALDNER, M. J. Telomerase deficiency reflects age-associated changes in CD4+ T cells. Immunity and Ageing, v. 19, n. 1, 1 dez. 2022.

MEDITZ, A. L.; HAAS, M. K.; FOLKVORD, J. M.; MELANDER, K.; YOUNG, R.; MCCARTER, M.; MAWHINNEY, S.; CAMPBELL, T. B.; LIE, Y.; COAKLEY, E.; LEVY, D. N.; CONNICK, E. HLA-DR + CD38 + CD4 + T Lymphocytes Have Elevated CCR5 Expression and Produce the Majority of R5-Tropic HIV-1 RNA In Vivo . Journal of Virology, v. 85, n. 19, p. 10189–10200, out. 2011.

MEIEROVICS, A.; YANKELEVICH, W. J. C.; COWLEY, S. C. MAIT cells are critical for optimal mucosal immune responses during in vivo pulmonary bacterial infection. Proceedings of the National Academy of Sciences of the United States of America, v. 110, n. 33, 13 ago. 2013.

MIURA, N.; HORIKAWA, I.; NISHIMOTO, A.; OHMURA, H.; ITO, H.; HIROHASHI, S.; SHAY, J. W.; OSHIMURA, M. Progressive Telomere Shortening and Telomerase Reactivation During Hepatocellular Carcinogenesis. Cancer Genet Cytogenet .93(1):56-62; 1997.

MOLINA-MOLINA, M.; BORIE, R. Clinical implications of telomere dysfunction in lung fibrosis. Current Opinion in Pulmonary Medicine, v. 24, n. 5, p. 440–444, 2018.

NAIKAWADI, R. P.; DISAYABUTR, S.; MALLAVIA, B.; DONNE, M. L.; GREEN, G.; LA, J. L.; ROCK, J. R.; LOONEY, M. R.; WOLTERS, P. J. Telomere dysfunction in alveolar epithelial cells causes lung remodeling and fibrosis. JCI Insight, v. 1, n. 14, 8 set. 2016.

NASEEM, S.; HUSSAIN, T.; MANZOOR, S. Interleukin-6: A promising cytokine to support liver regeneration and adaptive immunity in liver pathologiesCytokine and Growth Factor ReviewsElsevier Ltd, 1 fev. 2018.

NGUYEN, K. T. T. T.; WONG, J. M. Y. Telomerase biogenesis and activities from the perspective of its direct interacting partnersCancersMDPI AG, 1 jun. 2020.

NIEHAUS, C. E.; STRUNZ, B.; CORNILLET, M.; FALK, C. S.; SCHNIEDERS, A.; MAASOUMY, B.; HARDTKE, S.; MANNS, M. P.; KRAFT, A. R. M.; BJÖRKSTRÖM, N. K.; CORNBERG, M. MAIT Cells Are Enriched and Highly Functional in Ascites of Patients With Decompensated Liver Cirrhosis. Hepatology, v. 72, n. 4, 2020.

NOVAK, J.; DOBROVOLNY, J.; NOVAKOVA, L.; KOZAK, T. The Decrease in Number and Change in Phenotype of Mucosal-Associated Invariant T cells in the Elderly and Differences in Men and Women of Reproductive Age. Scandinavian Journal of Immunology, v. 80, n. 4, p. 271–275, 2014.

NOVO, E.; CANNITO, S.; ZAMARA, E.; DI BONZO, L. V.; CALIGIURI, A.; CRAVANZOLA, C.; COMPAGNONE, A.; COLOMBATTO, S.; MARRA, F.; PINZANI, M.; PAROLA, M. Proangiogenic cytokines as hypoxia-dependent factors stimulating migration of human hepatic stellate cells. American Journal of Pathology, v. 170, n. 6, p. 1942–1953, 2007.

PAIVA, R. M. A.; CALADO, R. T. Telomere dysfunction and hematologic disorders. *Em*: Progress in Molecular Biology and Translational Science. [s.l.] Elsevier B.V., 2014. p. 133–157.

PALM, W.; DE LANGE, T. How shelterin protects mammalian telomeresAnnual Review of Genetics. 2008.

PANGRAZZI, L.; MERYK, A.; NAISMITH, E.; KOZIEL, R.; LAIR, J.; KRISMER, M.; TRIEB, K.; GRUBECK-LOEBENSTEIN, B. “Inflamm-aging” influences immune cell survival factors in human bone marrow. European Journal of Immunology, v. 47, n. 3, p. 481–492, 1 mar. 2017.

PAUN, A.; BERGERON, M. E.; HASTON, C. K. The Th1/Th17 balance dictates the fibrosis response in murine radiation-induced lung disease. Scientific Reports, v. 7, n. 1, 1 dez. 2017.

PERRI, R. E.; LANGER, D. A.; CHATTERJEE, S.; GIBBONS, S. J.; GADGIL, J.; CAO, S.; FARRUGIA, G.; SHAH, V. H. Defects in cGMP-PKG pathway contribute to impaired NO-dependent responses in hepatic stellate cells upon activation. Am J Physiol Gastrointest Liver Physiol, v. 290, p. 535–542, 2006.

PETRASEK, J.; BALA, S.; CSAK, T.; LIPPAI, D.; KODYS, K.; MENASHY, V.; BARRIEAU, M.; MIN, S. Y.; KURT-JONES, E. A.; SZABO, G. IL-1 receptor antagonist ameliorates inflammasome-dependent alcoholic steatohepatitis in mice. Journal of Clinical Investigation, v. 122, n. 10, p. 3476–3489, 1 out. 2012.

PIÑEIRO-HERMIDA, S.; AUTILIO, C.; MARTÍNEZ, P.; BOSCH, F.; PÉREZ-GIL, J.; BLASCO, M. A. Telomerase treatment prevents lung profibrotic pathologies associated with physiological aging. Journal of Cell Biology, v. 219, n. 10, 1 ago. 2020.

PLENTZ, R. R.; CASELITZ, M.; BLECK, J. S.; GEBEL, M.; FLEMMING, P.; KUBICKA, S.; MANNS, M. P.; RUDOLPH, K. L. Hepatocellular telomere shortening correlates with chromosomal instability and the development of human hepatoma. Hepatology, v. 40, n. 1, p. 80–86, jul. 2004.

POVEDANO, J. M.; MARTINEZ, P.; FLORES, J. M.; MULERO, F.; BLASCO, M. A. Mice with Pulmonary Fibrosis Driven by Telomere Dysfunction. Cell Reports, v. 12, n. 2, p. 286–299, 14 jul. 2015.

QUINTELIER, K.; COUCKUYT, A.; EMMANEEL, A.; AERTS, J.; SAEYS, Y.; VAN GASSEN, S. Analyzing high-dimensional cytometry data using FlowSOMNature ProtocolsNature Research, 1 ago. 2021.

REISSING, J.; BERRES, M.; STRNAD, P.; WREE, A.; INZAUGARAT, M. E.; TRAUTWEIN, C.; BRUNS, T.; ZIMMERMANN, H. W. Th2 Cell Activation in Chronic Liver Disease Is Driven by Local IL33 and Contributes to IL13-Dependent Fibrogenesis. Cellular and Molecular Gastroenterology and Hepatology, v. 17, n. 4, p. 517–538, 2024.

RUDOLPH, K.L.; CHANG, S.; MILLARD, M.; SCHREIBER-AGUS, N.; DEPINHO, R.A. Inhibition of experimental liver cirrhosis in mice by telomerase gene delivery. Science. v. 287, n. 5456, p. 1253-1258; 2000.

SANDLER, N. G.; MENTINK-KANE, M. M.; CHEEVER, A. W.; WYNN, T. A. Global Gene Expression Profiles During Acute Pathogen-Induced Pulmonary Inflammation Reveal Divergent Roles for Th1 and Th2 Responses in Tissue Repair. The Journal of Immunology. 171(7):3655-67; 2003.

SAVAGE, S. A. Beginning at the ends: Telomeres and human disease. F1000Research F1000 Research Ltd, 2018.

SCHOLTEN, D.; TREBICKA, J.; LIEDTKE, C.; WEISKIRCHEN, R. The carbon tetrachloride model in mice. Laboratory Animals, v. 49, p. 4–11, 2015.

SCHWARTZ, C.; FALLON, P. G. Schistosoma “Eggs-iting” the host: Granuloma formation and egg excretionFrontiers in Immunology. Frontiers Media S.A., 1 out. 2018.

SEMPOWSKI, G. D.; HALE, L. P.; SUNDY, J. S.; MASSEY, J. M.; KOUP, R. A.; DOUEK, D. C.; PATEL, D. D.; HAYNES, B. F. Leukemia Inhibitory Factor, Oncostatin M, IL-6, and Stem Cell Factor mRNA Expression in Human Thymus Increases with Age and Is Associated with Thymic Atrophy . The Journal of Immunology. 2000.

SHAY, J. W.; WRIGHT, W. E. Telomeres and telomerase: three decades of progress. Nature Reviews Genetics, v. 20, n. 5, p. 299–309, 1 maio 2019.

SISSON, T. H.; MENDEZ, M.; CHOI, K.; SUBBOTINA, N.; COUREY, A.; CUNNINGHAM, A.; DAVE, A.; ENGELHARDT, J. F.; LIU, X.; WHITE, E. S.; THANNICKAL, V. J.; MOORE, B. B.; CHRISTENSEN, P. J.; SIMON, R. H. Targeted injury of type II alveolar epithelial cells induces pulmonary fibrosis. American Journal of Respiratory and Critical Care Medicine, v. 181, n. 3, p. 254–263, 1 fev. 2010.

SZIKSZ, E.; PAP, D.; LIPPAI, R.; BÉRES, N. J.; FEKETE, A.; SZABÓ, A. J.; VANNAY, Á. Fibrosis Related Inflammatory Mediators: Role of the IL-10 Cytokine FamilyMediators of Inflammation Hindawi Publishing Corporation, 2015.

TANG, X.-Z.; JO, J.; TAN, A. T.; SANDALOVA, E.; CHIA, A.; TAN, K. C.; LEE, K. H.; GEHRING, A. J.; DE LIBERO, G.; BERTOLETTI, A. IL-7 Licenses Activation of Human Liver Intrasinusoidal Mucosal-Associated Invariant T Cells. The Journal of Immunology, v. 190, n. 7, p. 3142–3152, 1 abr. 2013.

TAURA, K.; DE MINICIS, S.; SEKI, E.; HATANO, E.; IWAISAKO, K.; OSTERREICHER, C. H.; KODAMA, Y.; MIURA, K.; IKAI, I.; UEMOTO, S.; BRENNER, D. A. Hepatic Stellate Cells Secrete Angiopoietin 1 That Induces Angiogenesis in Liver Fibrosis. Gastroenterology, v. 135, n. 5, p. 1729–1738, 2008.

THABUT, D.; ROUTRAY, C.; LOMBERK, G.; SHERGILL, U.; GLASER, K.; HUEBERT, R.; PATEL, L.; MASYUK, T.; BLECHACZ, B.; VERCNOCKE, A.; RITMAN, E.; EHMAN, R.; URRUTIA, R.; SHAH, V. Complementary vascular and matrix regulatory pathways underlie the beneficial mechanism of action of sorafenib in liver fibrosis. Hepatology. 2011.

THIERINGER, F.; MAASS, T.; CZOCHRA, P.; KLOPCIC, B.; CONRAD, I.; FRIEBE, D.; SCHIRMACHER, P.; LOHSE, A. W.; BLESSING, M.; GALLE, P. R.; TEUFEL, A.; KANZLER, S. Spontaneous hepatic fibrosis in transgenic mice overexpressing PDGF-A. Gene, v. 423, n. 1, p. 23–28, 15 out. 2008.

TRAVES, S. L.; TUDHOPE, S. J.; FENWICK, P. S.; BELCHAMBER, K. B. R.; RUSSELL, R. E. K.; BARNES, P. J.; DONNELLY, L. E. Enhanced monocyte migration to CXCR3 and CCR5 chemokines in COPD Claudia Costa1. European Respiratory Journal, v. 47, n. 4, p. 1093–1102, 1 abr. 2016.

TSOCHATZIS, E. A.; BOSCH, J.; BURROUGHS, A. K. Liver cirrhosis. Em: The Lancet, 9930., 2014, [...]. Elsevier B.V., 2014. v. 383, p. 1749–1761.

TULJAPURKAR, S. R.; MCGUIRE, T. R.; BRUSNAHAN, S. K.; JACKSON, J. D.; GARVIN, K. L.; KESSINGER, M. A.; LANE, J. T.; O'KANE, B. J.; SHARP, J. G. Changes in human bone marrow fat content associated with changes in hematopoietic stem cell numbers and cytokine levels with aging. Journal of Anatomy, v. 219, n. 5, p. 574–581, nov. 2011.

VIALLARD, J. F.; BLOCH-MICHEL, C.; NEAU-CRANSAC, M.; TAUPIN, J. L.; GARRIGUE, S.; MIOSSEC, V.; MERCIE, P.; PELLEGRIN, J. L.; MOREAU, J. F. HLA-DR expression on lymphocyte subsets as a marker of disease activity in patients with systemic lupus erythematosus. Blackwell Science. 2001.

WAGNER, C. L.; HANUMANTHU, V. S.; CONOVER TALBOT, C.; ABRAHAM, R. S.; HAMM, D.; GABLE, D. L.; KANAKRY, C. G.; APPLEGATE, C. D.; SILICIANO, J.; BROOKS JACKSON, J.; DESIDERIO, S.; ALDER, J. K.; LUZNIK, L.; ARMANIOS, M. Short telomere syndromes cause a primary T cell immunodeficiency. Journal of Clinical Investigation, v. 128, n. 12, p. 5222–5234, 3 dez. 2018.

WANDERLEY, C. W.; COLÓN, D. F.; LUIZ, J. P. M.; OLIVEIRA, F. F.; VIACAVA, P. R.; LEITE, C. A.; PEREIRA, J. A.; SILVA, C. M.; SILVA, C. R.; SILVA, R. L.; SPECK-HERNANDEZ, C. A.; MOTA, J. M.; ALVES-FILHO, J. C.; LIMA-JUNIOR, R. C.; CUNHA, T. M.; CUNHA, F. Q. Paclitaxel reduces tumor growth by reprogramming tumor-associated macrophages to an M1 profile in a TLR4-dependent manner. Cancer Research, v. 78, n. 20, p. 5891–5900, 15 out. 2018.

WELLS, R. G.; KRUGLOV, E.; DRANOFF, J. A. Autocrine release of TGF-β by portal fibroblasts regulates cell growth. FEBS Letters, v. 559, n. 1–3, p. 107–110, 13 fev. 2004.

WIEMANN, S. U.; SATYANARAYANA, A.; TSAHURIDU, M.; TILLMANN, H. L.; ZENDER, L.; KLEMPNAUER, J.; FLEMMING, P.; FRANCO, S.; BLASCO, M. A.; MANNS, M. P.; RUDOLPH, K. L. Hepatocyte telomere shortening and senescence are general markers of human liver cirrhosis. FASEB J.16(9):935-42; 2002.

WU, X. Q.; YANG, Y.; LI, W. X.; CHENG, Y. H.; LI, X. F.; HUANG, C.; MENG, X. M.; WU, B. M.; LIU, X. H.; ZHANG, L.; LV, X. W.; LI, J. Telomerase reverse transcriptase acts in a feedback loop with NF-? B pathway to regulate macrophage polarization in alcoholic liver disease. Scientific Reports, v. 6, 4 jan. 2016.

WYNN, T. A. Cellular and molecular mechanisms of fibrosis. Journal of Pathology. 2008.

WYNN, T. A. Integrating mechanisms of pulmonary fibrosis. Journal of Experimental Medicine, v. 208, n. 7, p. 1339–1350, 4 jul. 2011.

YAO LAN, H.; KA, L.; LAN, H. Y.; KA SHING, L. Diverse Roles of TGF-β/Smads in Renal Fibrosis and Inflammation. Int. J. Biol. Sci, v. 7, n. 7, 2011.

YING, W.; CHERUKU, P. S.; BAZER, F. W.; SAFE, S. H.; ZHOU, B. Investigation of macrophage polarization using bone marrow derived macrophages. Journal of visualized experiments : JoVE, n. 76, 2013.

ZHANG, B. B.; YAN, C.; FANG, F.; DU, Y.; MA, R.; LI, X. Y.; YU, Q.; MENG, D.; TANG, R. X.; ZHENG, K. Y. Increased hepatic Th2 and Treg subsets are associated with biliary fibrosis in different strains of mice caused by Clonorchis sinensis. PLoS ONE, v. 12, n. 2, 1 fev. 2017.

ZHOU, W. C.; ZHANG, Q. B.; QIAO, L. Pathogenesis of liver cirrhosis. World Journal of Gastroenterology, v. 20, n. 23, p. 7312–7324, 21 jun. 2014.

ATTACHMENTS

ATTACHMENT A – Ethics Committee Approval (Animals)

UNIVERSIDADE DE SÃO PAULO
FACULDADE DE MEDICINA DE RIBEIRÃO PRETO
COMISSÃO DE ÉTICA NO USO DE ANIMAIS

CEUA FMRP-USP Comissão de Ética no Uso de Animais Replacement Reduction Refinement

FMRP 65 anos USP

A U T O R I Z A Ç Ã O

A CEUA-FMRP autoriza a execução do projeto intitulado: ***"Mecanismos imunes nas fibroses hepática e pulmonar associadas a telomeropatias em modelo murino e doença humana"***, registrado com o número do protocolo **244/2019**, sob a responsabilidade do **Prof. Dr. Rodrigo do Tocantins Calado de Saloma Rodrigues,** envolvendo a produção, manutenção ou utilização de animais pertencentes ao *filo Chordata, subfilo Vertebrata* (exceto humanos) para fins de pesquisa científica (ou ensino), encontra-se de acordo com os preceitos da Lei nº 11.794 de 8 de outubro de 2008, do Decreto nº 6.899 de 15 de julho de 2009 e com as normas editadas pelo Conselho Nacional de Controle de Experimentação Animal (CONCEA). O Protocolo foi **APROVADO *ad referendum*** pela Comissão de Ética no Uso de Animais da Faculdade de Medicina de Ribeirão Preto da Universidade de São Paulo, em 08 de junho de 2020.

Colaborador: Willian Róbert Gomes

Lembramos da obrigatoriedade do Relatório Final, em modelo da CEUA, para emissão do Certificado, como disposto nas Resoluções Normativas do CONCEA.

Finalidade		() Ensino (X) Pesquisa Científica		
Vigência da autorização		08/06/2020 a 13/02/2025		
Espécie/Linhagem	Nº de Animais	Peso/Idade	Sexo	Origem
Camundongo / Terc	40	25g / 60 dias	Macho	Laboratório de Estudos Experimentais em Animais (LEEA)
Camundongo / Tert	40	25g / 60 dias		Laboratório de Estudos Experimentais em Animais (LEEA)
Camundongo / c57bl6/j	40	25g / 60 dias		Laboratório de Estudos Experimentais em Animais (LEEA)

Ribeirão Preto, 01 de abril de 2020

Profa. Dra. Katiuchia Uzzun Sales
Coordenadora da CEUA–FMRP–USP

Faculdade de Medicina de Ribeirão Preto - USP - Av. Bandeirantes, 3900 - Ribeirão Preto - SP - Brasil -14049-900 - Tel.: (16) 3315-3301 / 3315.3275 - e-mail: ceua@fmrp.usp.br

ATTACHMENT B – Ethics Committee Approval (Humans)

COMISSÃO NACIONAL DE
ÉTICA EM PESQUISA

Continuação do Parecer: 4.164.097

/ Brochura Investigador	pdf	11:24:40	Gomes	Aceito
TCLE / Termos de Assentimento / Justificativa de Ausência	TCLE_PACIENTE.pdf	22/01/2020 14:41:44	Willian Robert Gomes	Aceito
TCLE / Termos de Assentimento / Justificativa de Ausência	TCLE_CONTROLE.pdf	22/01/2020 14:41:34	Willian Robert Gomes	Aceito
Projeto Detalhado / Brochura Investigador	Projeto_Doutorado_Willian.pdf	22/01/2020 14:41:20	Willian Robert Gomes	Aceito
Cronograma	Cronograma_de_execucao.pdf	22/01/2020 11:00:35	Willian Robert Gomes	Aceito
Orçamento	Orcamento_WRG.pdf	22/01/2020 10:24:37	Willian Robert Gomes	Aceito
Outros	Aprovacao_UPC.pdf	22/01/2020 10:21:14	Willian Robert Gomes	Aceito
Outros	Criacao_Biorrepositorio.pdf	22/01/2020 10:20:49	Willian Robert Gomes	Aceito

Situação do Parecer:
Aprovado

BRASILIA, 20 de Julho de 2020

Assinado por:
Jorge Alves de Almeida Venancio
(Coordenador(a))

Endereço: SRTVN 701, Via W 5 Norte, lote D - Edifício PO 700, 3º andar
Bairro: Asa Norte **CEP:** 70.719-040
UF: DF **Município:** BRASILIA
Telefone: (61)3315-5877 **E-mail:** conep@saude.gov.br